

NUMERICAL PORTRAIT OF A RELATIVISTIC THIN FILM BCS SUPERFLUID

Simon Hands^a, Biagio Lucini^b and Susan Morrison^a

^a*Department of Physics, University of Wales Swansea,
Singleton Park, Swansea SA2 8PP, U.K.*

^b*Department of Theoretical Physics, 1 Keble Road, Oxford OX1 3NP, U.K.*

Abstract

We present results of numerical simulations of the 2+1d Nambu – Jona-Lasinio model with a non-zero baryon chemical potential μ including the effects of a diquark source term. Diquark condensates, susceptibilities and masses are measured as functions of source strength j . The results suggest that diquark condensation does not take place in the high density phase $\mu > \mu_c$, but rather that the condensate scales non-analytically with j implying a line of critical points and long range phase coherence. Analogies are drawn with the low temperature phase of the 2d XY model. The spectrum of the spin- $\frac{1}{2}$ sector is also studied yielding the quasiparticle dispersion relation. There is no evidence for a non-zero gap; rather the results are characteristic of a normal Fermi liquid with Fermi velocity less than that of light. We conclude that the high density phase of the model describes a relativistic gapless thin film BCS superfluid.

PACS: 11.10.Kk, 11.30.Fs, 11.15.Ha, 21.65.+f, 67.70.+n

Keywords: Monte Carlo simulation, chemical potential, diquark condensate, superfluidity

1 Introduction

Spontaneous symmetry breaking in particle physics was pre-dated by the Bardeen-Cooper-Schrieffer (BCS) mechanism for superconductivity in metals at low temperature [1], which predicts a ground state in which a macroscopic fraction of the electrons in the vicinity of the Fermi surface reside in spin-0 bound states known as Cooper pairs. In field theoretic terms [2] the Cooper pairs form a condensate which alter the symmetry of the ground state; in the case of superconductivity U(1) electromagnetic gauge invariance is spontaneously broken, leading to the Meissner effect, ie. exclusion of magnetic field from a superconducting sample due to surface screening currents. The ideas of BCS have been incorporated into particle physics in two distinct directions. Firstly, particle – anti-particle pair condensation $\langle \bar{\psi}\psi \rangle \neq 0$ was suggested as a means of breaking the global chiral symmetries responsible for keeping fermion masses small; Goldstone’s theorem then predicts light weakly-interacting bosonic states which can be identified with pions, whose masses are considerably less than the nucleon, the lightest strongly-interacting fermion. The resulting model provides a reasonable description of low-energy strong-interaction phenomena [3]. Secondly, condensation of an elementary Higgs field has of course been invoked as a mechanism for electroweak gauge symmetry breaking, imbuing gauge bosons (as well as fermionic matter fields) with non-zero mass in precise analogy with the Meissner effect.

In recent years the BCS mechanism has returned to particle physics in a new guise in the context of the fundamental theory of the strong interaction, QCD, at high density. For baryon charge densities $n_B \sim O(1)\text{fm}^{-3}$, it is believed that chiral symmetry is restored and nucleons dissociate into quarks. The resulting ground state is thought to be *quark matter* in which to first approximation the dominant degrees of freedom are relativistic degenerate quarks forming a Fermi sphere with Fermi momentum $k_F \approx 350 - 400\text{MeV}$. Such conditions are conceivably found in the cores of neutron stars. However, since the force between quarks due to eg. one-gluon exchange is attractive, this simple picture is unstable with respect to a BCS scenario in which condensation of *diquark pairs* occurs [4]. Since the qq wavefunction is gauge non-singlet, the resulting ground state renders some or all of the gluons massive, an effect known as “color superconductivity”. The resulting dynamically generated mass scale or “gap” Δ is predicted to be $O(100)\text{MeV}$ [5], and hence comparable with the constituent quark scale.

Unfortunately, theoretical studies of color superconductivity are to date limited

to perturbative and self-consistent methods [4, 5, 6]; there is no systematic method of performing non-perturbative QCD calculations in the high density regime because of the notorious “sign problem”, ie. the measure of the Euclidean path integral becomes complex once baryon chemical potential $\mu \neq 0$, making the importance sampling techniques traditionally used in numerical simulations of lattice gauge theory ineffective. There are, however, strongly-interacting model field theories where this difficulty can be circumvented. One is QCD with just two colors, in which qq baryons and $q\bar{q}$ mesons fall into multiplets related by enhanced global symmetries. Some of the multiplets contain Goldstone bosons, so that the methods of chiral perturbation theory can be applied [7]. Baryonic matter $n_B > 0$ forms for chemical potential $\mu \gtrsim m_\pi/2$ [7, 8, 9]. The resulting ground state is a superfluid of light but strongly bound qq states which form a Bose-Einstein condensate. There is no Fermi surface in this regime, and the BCS description is inappropriate.

Another possibility, to be studied in the present paper, are four-fermi models such as the Nambu – Jona-Lasinio (NJL) model [3], in which it can be shown that the effects of adding “conjugate quarks” q^c to make the path integral real and positive have little impact on the physics: at low density light Goldstone states arising as a result of chiral symmetry breaking can only form in mesonic $q\bar{q}$ channels, whereas baryonic qq^c bound states remain massive, ie. at the constituent quark scale [10]. This means that unlike in physical three-color QCD with conjugate quarks, it is possible for simulations of four-fermi models to maintain a separation of scales between m_π and the critical μ_c at which chiral symmetry is restored and baryonic matter induced into the ground state [11]. In this case the model does not reproduce any of the physics of confinement, but has a Fermi surface for $n_B > 0$.

Because the qq interaction is attractive, diquark condensation is expected in the high density phase of each of the models described above. In both cases, however, the relevant $\langle qq \rangle \neq 0$ is gauge singlet, meaning that the ground state is not superconducting, but rather *superfluid*. In field theoretic terms, a superfluid forming by BCS condensation is characterised by a ground state which does not respect a global symmetry of the underlying action, in this case the U(1) corresponding to baryon number, which is thus no longer a good quantum number. Fermionic excitations above the Fermi surface are a superposition of particle and hole states, and require energy $\geq \Delta$ to excite. Finally, because a continuous global symmetry is spontaneously broken, Goldstone’s theorem applies and massless diquark states are expected in the excitation spectrum. Physically these result both in a long-ranged interaction between

the vortex excitations found in a rotating superfluid, and in propagating waves of temperature variation known as *second sound* [12, 13].

The two known superfluids are liquid ^4He at kelvin and liquid ^3He at milli-kelvin temperatures. ^4He is a boson and is naturally treated using a complex scalar field theory, superfluidity arising via a Bose-Einstein condensation. Note, however, that a fundamental description would treat ^4He as a tightly-bound state of fermionic constituents, not too dissimilar in spirit to Two-Color QCD. ^3He by contrast is a fermion, and superfluidity in this case is believed to arise via a BCS instability resulting in a condensation of weakly-bound Cooper pairs. We might thus consider superfluidity in the NJL model as a relativistic generalisation of this phenomenon. It is important to note, though, that due to short distance repulsion between helium atoms the BCS wavefunction in ^3He is actually p -wave, resulting in ground states described by a complicated order parameter and many interesting topological excitations [14]. In the NJL model studied here, the corresponding qq wavefunction is a scalar s -wave, and any superfluid might be expected to behave more like ^4He .

Superfluidity in a relativistic model similar to the NJL model has been studied using mean field techniques in [6]. In our previous work [15, 16] we have attempted to identify superfluidity in the $2+1d$ NJL model using non-perturbative numerical lattice simulations. Apart from the obvious computational gain, we chose this particular dimensionality because the model has a non-trivial continuum limit [17, 18]. Therefore, in contrast to effective descriptions such as the Landau-Ginzburg theory, the condensed matter described in this approach is formed from the elementary quanta of an interacting field theory. Our results have not supported the expected scenario outlined above, raising the question of whether important physics is neglected in the self-consistent approach. Although there is evidence for enhanced diquark pairing in the scalar isosinglet channel in [15], we have not succeeded in finding an unambiguous signal for a condensate $\langle qq \rangle \neq 0$. Rather, in the high density phase the condensate appears to vanish non-analytically as a function of diquark source strength j , suggesting critical behaviour [16]. Studies of the excitation spectrum in the spin- $\frac{1}{2}$ sector reveal a sharp Fermi surface and no evidence for a gap $\Delta \neq 0$ [16]. The purpose of the present paper is to present these results in greater depth, and to attempt to interpret them. As we shall see, it may be possible to attribute the unconventional signals to the specifically two-dimensional nature of the system being studied, which thus bears many resemblances to superfluidity observed in thin helium films [19]. We will argue that neither long range order $\langle qq \rangle \neq 0$ nor a gap $\Delta \neq 0$ are necessary attributes of

a superfluid. Instead, the critical behaviour observed in [16] results from long range *coherence* in the phase of the diquark wavefunction, which appears to be a sufficient condition for thin film superfluidity [20].

In Sec. 2 we review the formulation and numerical simulation of the lattice NJL model in $2+1d$ with non-zero chemical potential μ , paying particular attention to the introduction of diquark source terms jqq via the use of a *Gor'kov basis* [2]. It is thus possible to define diquark observables which are measurable on a finite system; Sec. 3 reviews numerical results for the diquark condensate $\langle qq(j) \rangle$, the associated susceptibilities, and diquark masses. Critical behaviour in the high density phase $n_B > 0$ is identified after extrapolating results for the first two quantities to the zero-temperature (ie. $L_t \rightarrow \infty$) limit, leading to consistent estimates for the critical exponent conventionally denoted δ which vary with μ . In Sec. 4 this behaviour is discussed in analogy with that of the $2d$ XY model, in which long range order is washed out by spin wave excitations and which also displays critical behaviour in a continuous parameter range. It is argued that in such circumstances persistent flow, the defining property of a superfluid, can only be disrupted by excitations costing infinite energy in the thermodynamic limit. Sec. 5 presents the results of a study of the dispersion relation $E(k)$ of spin- $\frac{1}{2}$ *quasiparticle* excitations in the dense phase, revealing a sharp Fermi surface for the first time using lattice methods. There is no evidence for particle-hole mixing or a non-vanishing gap as the source strength $j \rightarrow 0$. Instead, the results in this sector are consistent with a normal Fermi liquid of the type first discussed by Landau [21, 22]; in particular it is possible to estimate both Fermi momentum k_F and velocity β_F as functions of μ and to show that these depart from their free-field values, yielding information on quasiparticle interactions. Conclusions and suggestions for further work are outlined in Sec. 6

2 The Lattice Model

2.1 Formulation and Symmetries

The model studied in this paper is a lattice transcription of the NJL model in $2+1$ dimensions, identical to that studied in [15, 16]. It is defined by the Euclidean action

$$S = S_{fer} + S_{bos} \quad ; \quad S_{fer} = \sum_x \bar{\chi} M[\Phi] \chi + j \chi^{tr} \tau_2 \chi + \bar{j} \bar{\chi} \tau_2 \bar{\chi}^{tr} \quad ; \quad S_{bos} = \frac{1}{g^2} \sum_{\tilde{x}} \text{tr} \Phi^\dagger \Phi, \quad (2.1)$$

where $\chi, \bar{\chi}$ are isospinor fermionic fields defined on the sites x of a $2+1d$ lattice, and $\Phi \equiv \sigma + i\vec{\pi} \cdot \vec{\tau}$ is a 2×2 matrix of bosonic auxiliary fields living on the dual sites \tilde{x} . The kinetic operator M has the standard form for staggered lattice fermions interacting with scalar fields [18]:

$$M_{xy}^{pq}[\Phi] = \frac{1}{2}\delta^{pq} \left[(e^\mu \delta_{yx+\hat{0}} - e^{-\mu} \delta_{yx-\hat{0}}) + \sum_{\nu=1,2} \eta_\nu(x) (\delta_{yx+\hat{\nu}} - \delta_{yx-\hat{\nu}}) + 2m\delta_{xy} \right] + \frac{1}{8}\delta_{xy} \sum_{\langle \tilde{x}, x \rangle} \left(\sigma(\tilde{x})\delta^{pq} + i\varepsilon(x)\vec{\pi}(\tilde{x}) \cdot \vec{\tau}^{pq} \right). \quad (2.2)$$

The parameters are bare fermion mass m , baryon chemical potential μ , and coupling g^2 . The $\vec{\tau}$ are Pauli matrices normalised to $\text{tr}(\tau_i \tau_j) = 2\delta_{ij}$ acting on isopin indices $p, q = 1, 2$. The symbols $\eta_\nu(x)$ denote the phases $(-1)^{x_0+\dots+x_{\nu-1}}$, $\varepsilon(x)$ the phase $(-1)^{x_0+x_1+x_2}$, and $\langle \tilde{x}, x \rangle$ the set of 8 dual sites neighbouring x . Integration over the auxiliary Φ fields leads to an equivalent action in terms of fermions which self-interact via a four-point contact term proportional to g^2 , corresponding to the interaction of the NJL model [23].

In addition to the usual NJL interactions, Eqn. (2.1) contains diquark and anti-diquark terms proportional to source strengths j and \bar{j} respectively. These have been introduced to enable the measurement of the diquark condensate $\langle \chi^{tr} \tau_2 \chi \rangle$ on a finite system, in precise analogy to the role of the bare mass m in the measurement of the chiral condensate $\langle \bar{\chi} \chi \rangle$. To proceed, we define the bispinor $\Psi^{tr} = (\bar{\chi}^{tr}, \chi)$, and rewrite the fermion action as a quadratic form $S_{fer} = \Psi^{tr} \mathcal{A} \Psi$, where in this Gor'kov basis the antisymmetric matrix \mathcal{A} is

$$\mathcal{A} = \begin{pmatrix} \bar{j}\tau_2 & \frac{1}{2}M \\ -\frac{1}{2}M^{tr} & j\tau_2 \end{pmatrix}. \quad (2.3)$$

The fermion fields may then be integrated out to yield the following Euclidean path integral:

$$Z = \int D\sigma D\vec{\pi} \text{Pf}(2\mathcal{A}[\Phi, j, \bar{j}]) \exp -S_{bos}[\Phi], \quad (2.4)$$

where the pfaffian $\text{Pf}(Q) \equiv \sqrt{\det Q}$. Note that this expression differs from the (incorrect) version given in [16] by a physically irrelevant factor of two; for convenience we will stick with the current notation, but note that if the source is interpreted as a Majorana mass λ , then $j = \lambda/2$ [9].

The model described by the action (2.1,2.2) has an $SU(2)_L \otimes SU(2)_R \otimes U(1)_B$ global symmetry. Defining projection operators $\mathcal{P}_{e/o} = \frac{1}{2}(1 \pm \varepsilon(x))$ onto even and odd

sublattices respectively, we have

$$\chi \mapsto (\mathcal{P}_e U + \mathcal{P}_o V)\chi; \quad \bar{\chi} \mapsto \bar{\chi}(\mathcal{P}_e V^\dagger + \mathcal{P}_o U^\dagger); \quad \Phi \mapsto V\Phi U^\dagger \quad [U, V \in \text{SU}(2)]: \quad (2.5)$$

$$\chi \mapsto e^{i\alpha}\chi; \quad \bar{\chi} \mapsto \bar{\chi}e^{-i\alpha} \quad [e^{i\alpha} \in \text{U}(1)_B]. \quad (2.6)$$

The symmetry (2.5) is broken to a diagonal $\text{SU}(2)_V$ of isospin with $U \equiv V$ in (2.5), either explicitly by a bare fermion mass $m \neq 0$, or spontaneously by the generation of a chiral condensate $\langle \bar{\chi}\chi \rangle \neq 0$ by the model's dynamics. For $\mu = 0$ this occurs for a sufficiently strong coupling $g^2 > g_c^2 \simeq 1.0a$, where a is the physical lattice spacing [18]. In the chirally broken phase the fermions have a dynamically generated mass $\Sigma \simeq \langle \sigma \rangle \equiv \frac{g^2}{2} \langle \bar{\chi}\chi \rangle$. Since $\Sigma a \rightarrow 0$ as $g^2 \rightarrow g_c^2$, a continuum limit may be taken at this critical point. A remarkable feature of the 2+1d NJL model is that the continuum theory so obtained remains interacting [17, 18]. As in our previous studies [15, 16], the simulations in this paper were performed with $g^2 = 2.0$ corresponding to $\Sigma a = 0.71$, implying that we are rather far from the continuum limit.

For $\mu \neq 0$ the model is known to exhibit a strong first-order transition to a chirally symmetric phase [24]; for our realisation this occurs at a critical $\mu_c \simeq \Sigma \simeq 0.65$, as shown in Fig 1 [15]. Chiral symmetry restoration is accompanied at this point by the onset of a non-vanishing density of baryon charge in the ground state, signalled by a condensate

$$n_B = \frac{1}{2V} \frac{\partial \ln Z}{\partial \mu} = \frac{1}{4} \langle \bar{\chi}(x)e^\mu \chi(x + \hat{0}) + \bar{\chi}(x)e^{-\mu} \chi(x - \hat{0}) \rangle > 0. \quad (2.7)$$

Existing numerical evidence suggests these two *a priori* distinct transitions are coincident [25]. For $\mu > \mu_c$, $\Sigma \simeq 0$, and the density follows the approximate form $n_B \propto \mu^2$, the behaviour expected for massless states populating a 2 dimensional Fermi sphere of radius $E_F = \mu$, until it gets close to its saturation value of one quark of each isospin per lattice site. For our realisation, $n_B \simeq 0.25$ quarks of each isospin label per site at $\mu = 0.8$, corresponding to a physical density of about 80 fm^{-2} assuming a constituent quark mass Σ of 300 MeV; by $\mu = 0.9$ this has risen to $n_B \simeq 0.4$, corresponding to 125 fm^{-2} .

The question which will occupy us in this paper is the nature of the high density phase present for $\mu > \mu_c$, and in particular whether the $\text{U}(1)_B$ symmetry (2.6) is spontaneously broken by the generation of a diquark condensate which we will generically denote by $\langle qq \rangle \neq 0$. In a BCS condensation, the participating diquark pairs come from the neighbourhood of the Fermi surface. The resulting ground state is

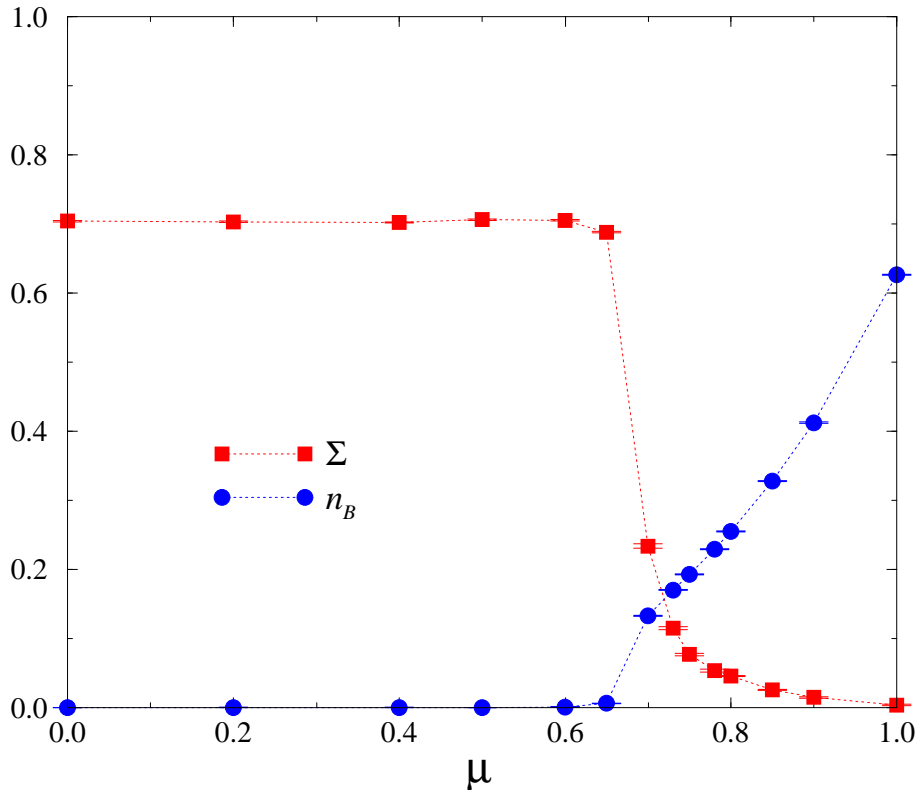


Figure 1: Chiral condensate Σ and baryon charge density n_B as a function of μ for a $16^2 \times 24$ system with $g^2 = 2.0$, $m = 0.01$, $j = 0$.

separated from excited states by an energy gap Δ analogous to the constituent quark mass Σ in a chirally-broken vacuum; mean-field calculations of a phenomenologically inspired $3+1d$ NJL-type model predict that for quark matter Δ is of the same order as Σ [5]. As well as being massive, the quasiparticle excitations above the ground state carry indefinite baryon charge due to the $U(1)_B$ breaking. Physically, this means that the quasiparticle is a coherent superposition of particle and hole states. In Ref. [15] diquark timeslice correlators $\sum_{\vec{x}} \langle qq(\vec{0}, 0) \bar{q}\bar{q}(\vec{x}, t) \rangle$ in various plausible condensation channels were studied for $\mu > \mu_c$, and evidence for pairing found, in the form of a plateau whose height did not decrease with Euclidean time separation t , for the scalar $SU(2)_L \otimes SU(2)_R$ singlet channel $qq = \chi^{tr} \tau_2 \chi$. However, the naive interpretation of diquark condensation via the clustering hypothesis, namely that

$$\lim_{t \rightarrow \infty} \langle qq(0) \bar{q}\bar{q}(t) \rangle = |\langle qq \rangle|^2, \quad (2.8)$$

was ruled out because the plateau height did not scale in the expected way, ie. exten-

sively in the spatial volume L_s^2 . To clarify the situation, Ref. [16] introduced diquark source terms, as in (2.1), making direct measurements of $\langle qq \rangle$ possible; we now review the ‘standard’ signals which might be expected if diquark condensation occurs.

Firstly we define diquark operators qq_{\pm} via

$$qq_{\pm}(x) = \frac{1}{2} \left[\chi^{tr}(x) \tau_2 \chi(x) \pm \bar{\chi}(x) \tau_2 \bar{\chi}^{tr}(x) \right], \quad (2.9)$$

with corresponding source strengths $j_{\pm} = j \pm \bar{j}$. It is readily checked that qq_{\pm} are invariant under $SU(2)_L \otimes SU(2)_R$ rotations (2.5), but rotate into each other under $U(1)_B$ (2.6). In terms of 4-component spinors ψ , the operators (2.9) may be written [15]

$$qq_{\pm} = -i \left[\psi^{tr} (\mathcal{C} \gamma_5 \otimes \tau_2 \otimes \tau_2) \psi \pm \bar{\psi} (\mathcal{C} \gamma_5 \otimes \tau_2 \otimes \tau_2) \bar{\psi}^{tr} \right], \quad (2.10)$$

where the first matrix in the tensor product acts on spinor indices, the second on a 2-component flavor structure which is implicit in the staggered fermion approach [26], and the third on the explicit isospin index introduced in (2.1). The charge conjugation matrix \mathcal{C} is defined by $\mathcal{C} \gamma_{\mu} \mathcal{C}^{-1} = -\gamma_{\mu}^*$. The diquark condensate is now given by

$$\langle qq_+ \rangle = \frac{1}{V} \frac{\partial \ln Z}{\partial j_+} = \frac{1}{4V} \langle \text{tr} \tau_2 \mathcal{A}^{-1} \rangle, \quad (2.11)$$

and is calculable using standard lattice techniques, such as the use of a stochastic estimator for the diagonal elements of the inverse matrix. The non-vanishing of (2.11) in the limit $j_+ \rightarrow 0$ is a criterion for the spontaneous breakdown of $U(1)_B$ symmetry. Furthermore, if we define susceptibilities

$$\chi_{\pm} = \sum_x \langle qq_{\pm}(0) qq_{\pm}(x) \rangle, \quad (2.12)$$

then it is straightforward to derive a Ward identity analogous to the axial Ward identity for the pion propagator:

$$\chi_- |_{j_-=0} = \frac{\langle qq_+ \rangle}{j_+}. \quad (2.13)$$

On the assumption that the dominant contribution to χ_- is from a simple pole, then qq_- couples to a Goldstone mode whose mass M_- vanishes in the zero source limit as $\sqrt{j_+}$. If we similarly attribute χ_+ to a ‘‘Higgs mode’’, then the ratio χ_+/χ_- provides an alternative means of distinguishing possible symmetry-breaking scenarios in the limit $j_+ \rightarrow 0$:

$$R = \lim_{j_+ \rightarrow 0} -\frac{\chi_+}{\chi_-} = \begin{cases} 1, & \text{if } U(1)_B \text{ manifest;} \\ 0, & \text{if } U(1)_B \text{ broken.} \end{cases} \quad (2.14)$$

In Sec. 3 we will present numerical results for these quantities and discuss to what extent the above considerations help in describing the high density phase of the 2+1d NJL model.

2.2 The Simulation

Numerical simulation of the path integral (2.4) requires some discussion of how to deal with the pfaffian. First let us find the condition that $\det 2\mathcal{A}$ is real. Using the property of a block square matrix

$$\det \begin{pmatrix} X & Y \\ W & Z \end{pmatrix} = \det X \det(Z - WX^{-1}Y), \quad (2.15)$$

and the property $\tau_2 M \tau_2 = M^*$ which follows from (2.2), we deduce

$$\det 2\mathcal{A} = \det(4j\bar{j} + M^\dagger M), \quad (2.16)$$

and is hence real and positive if $j\bar{j}$ is chosen real and positive. In all our work we choose $j = \bar{j}$ real which satisfies this condition. It follows that $\text{Pf}(2\mathcal{A})$ is real. In fact, one can go further and argue that it is also positive as follows. In the limit $j, \bar{j} \rightarrow 0$, $\text{Pf}(2\mathcal{A})$ reduces to $\det M$, which can be proven both real and positive using an argument, identical to that used for SU(2) lattice gauge theory with staggered quarks in the fundamental representation [8], showing that any complex eigenvalue of M is accompanied in the spectrum by its conjugate, and any purely real eigenvalue is doubly degenerate. Relation (2.16), however, shows that $\det 2\mathcal{A}$ can only increase and hence cannot change sign once $j\bar{j} > 0$; it follows that $\text{Pf}(2\mathcal{A})$ can be consistently chosen real and positive [9].

Despite this reassuring property, in our simulation we chose to use $\det^{\frac{1}{2}}(\mathcal{A}^\dagger \mathcal{A}) \propto \text{Pf}^2(2\mathcal{A})$ as the measure, corresponding to two staggered lattice fermion species, for consistency with the model of [15] which is recovered in the limit $j \rightarrow 0$. It can be shown that in the continuum limit the model contains $N_f = 4$ species of four-component Dirac fermions [26]. The simulation is performed using a hybrid molecular dynamics ‘‘R’’ algorithm [27], in which the square root is taken by inserting a factor of $\frac{1}{2}$ in the force term derived from a local action; note that we were able to debug and tune the code by also checking against an exact algorithm for the case $N_f = 8$. In all cases we used a molecular dynamics timestep $\Delta\tau = 0.04$, and never saw any evidence of departure from equipartition of energy. We performed simulations on lattice sizes $L_s^2 \times L_t = 16^3, 16^2 \times 24, 24^3, 32^3$, and in one case 48^3 , with the coupling

g^2 fixed to 2.0 as described above, and bare Dirac mass m fixed to 0.01 to assist with the identification of chirally broken and restored phases. A typical run is over $O(400)$ HMD time units with mean refreshment interval 1.0; data were taken every two units. The cost of the simulation rises considerably in the chirally-restored phase where the diagonal elements of M , proportional to $\langle\sigma\rangle$, are small, particularly as $j \rightarrow 0$. The 48^3 point at $\mu = 0.8, j = 0.025$ required approximately 40 SGI Origin2000 processor days.

In Sec. 3.1 we review the behaviour of the model as a function of μ , and present results for $\langle qq \rangle$ taken in the “partially quenched” approximation in which $j \neq 0$ only in the measurement, and the simulation performed using an exact algorithm with $j = 0$. Our studies with full pfaffian dynamics, presented in Secs. 3.2, 3.3 and 3.4, focussed on two representative points in the chirally symmetric low density phase at $\mu = 0.0, 0.2$, and on two values in the high density chirally symmetric phase $\mu = 0.8, 0.9$. We used $j = \bar{j}$ ranging in value from 0.3 down to 0.025. In our studies of the quasiparticle spectrum discussed in Sec. 5 we performed runs on 32^3 at 4 additional values of $\mu \in (0.8, 0.9)$.

3 Numerical Results for Diquark Observables

3.1 Partially Quenched Results

In this section we discuss the direct numerical measurement of diquark condensates $\langle qq \rangle$, which the Gor’kov basis discussed in the previous section makes possible. To warm up we consider the partially quenched approximation, in which the source strength j is set to zero in the updating of the $\{\Phi\}$ configuration, which thus proceeds via an exact Hybrid Monte Carlo algorithm as in [15], but is non-zero in the measurement routine so that $\langle qq \rangle$ can be measured via (2.11). Since at a given μ a single simulation serves for all j , this approach is fairly cheap and hence good coverage of the μ axis is practicable. Our results are shown in Fig. 2, where open symbols denote data taken in the low density phase $\mu < \mu_c$, and filled symbols are from the dense phase. For $\mu < \mu_c$ $\langle qq_+ \rangle$ varies approximately linearly with j , implying that a smooth extrapolation to the origin is possible, and hence the condensate vanishes in the $j \rightarrow 0$ limit. A striking jump occurs between $\mu = 0.65$ and $\mu = 0.7$, and for values of μ in the dense phase $\langle qq(j) \rangle$ is markedly more curved. This behaviour cannot be taken as evidence of diquark condensation, however; one should expect discontinuities in all physical observables on different sides of a first order phase transition. Despite

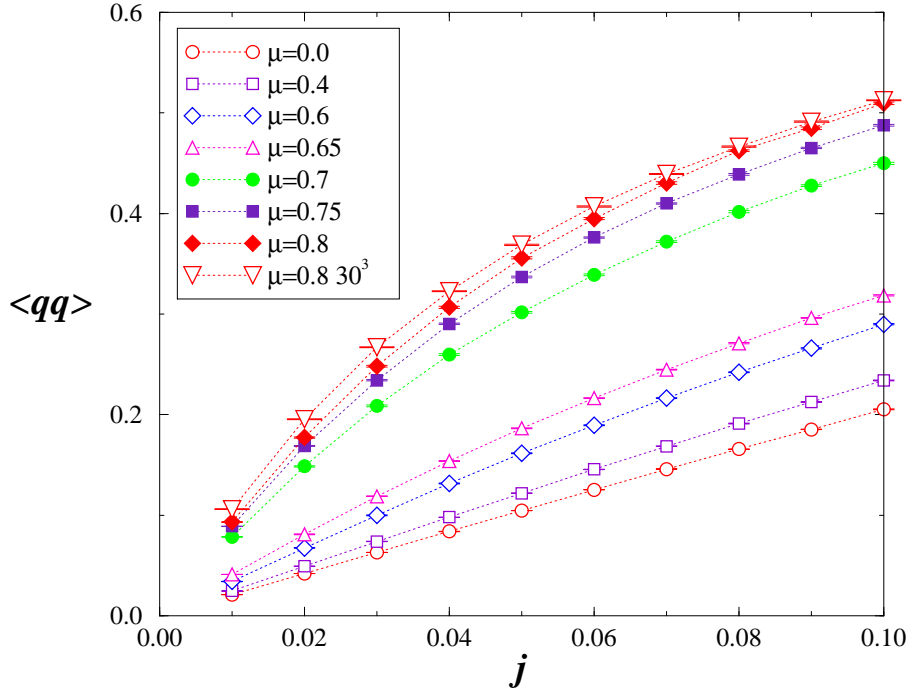


Figure 2: Partially quenched results for the diquark condensate $\langle \chi^{tr} \tau_2 \chi \rangle$ as a function of source strength j for various values of μ ; unless otherwise shown, data was taken on a $16^2 \times 24$ system.

the curvature of the lines a smooth extrapolation to the origin consistent with unbroken baryon number symmetry at high density is still plausible. Another possibility, suggested by the $\mu = 0.8$ data from a 30^3 lattice shown in Fig. 2, is that the symmetry breaking is masked by a finite-volume suppression as $j \rightarrow 0$. To explore the behaviour for $\mu > \mu_c$ in more depth data from lattices with several distinct L_s and L_t are needed. We chose to perform this using “unitary” data generated using the correct measure (2.4) for a limited number of different μ , as described next.

3.2 Diquark Condensate

In Fig. 3 we show $\langle qq_+ \rangle$ data taken from simulations using the full pfaffian measure (2.4) at two values of μ from each phase on a 32^3 lattice. The results resemble those of the partially quenched approach shown in Fig. 2 both qualitatively and quantitatively. The curvature of $\langle qq_+(j) \rangle$ in the dense phase seems to become more pronounced with increased μ , to the extent that by $j \simeq 0.2$ the results at $\mu = 0.9$ actually undershoot

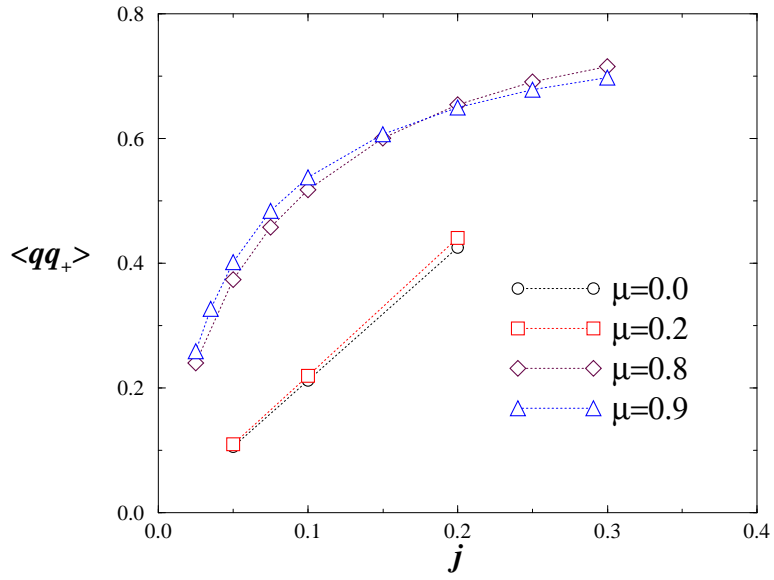


Figure 3: Results for $\langle qq_+ \rangle$ vs. j for various values of μ from a full simulation on a 32^3 system.

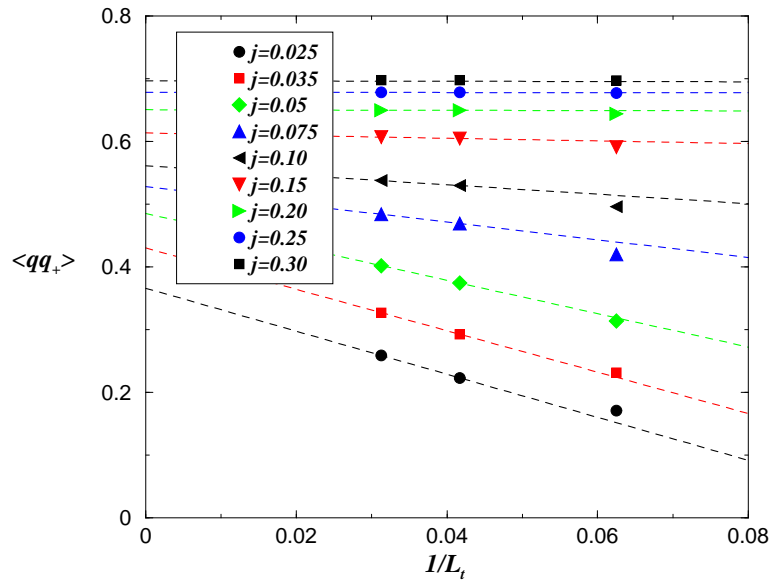


Figure 4: Extrapolation of $\langle qq_+ \rangle$ at $\mu = 0.9$ to the thermodynamic limit.

Table 1: Values of $\langle qq_+(j) \rangle$ on various lattice sizes at $\mu = 0.8$.

j	16^3	$16^2 \times 24$	24^3	32^3	48^3
0.025	0.1713(3)	0.2158(3)	0.2140(2)	0.2400(2)	0.2619(1)
0.035	0.2328(3)	—	0.2801(3)	—	—
0.05	0.3125(4)	0.3581(3)	0.3572(3)	0.3737(2)	—
0.075	0.4165(5)	0.4497(3)	0.4492(3)	0.4576(2)	—
0.1	0.4921(5)	0.5137(3)	0.5133(4)	0.5176(2)	—
0.15	0.5910(6)	0.5993(3)	0.6002(3)	0.6003(2)	—
0.2	0.6506(5)	0.6547(3)	0.6542(3)	0.6544(2)	—
0.25	0.6896(5)	0.6905(3)	0.6910(3)	0.6906(2)	—
0.3	0.7148(5)	0.7158(3)	0.7160(3)	0.7155(2)	—

those at $\mu = 0.8$. As remarked in the previous section, there are significant finite volume effects in this phase. Fig. 4 shows $\mu = 0.9$ data from simulations on 16^3 , 24^3 and 32^3 lattices. The equivalent data for $\mu = 0.8$, including a single point from 48^3 , is tabulated in Table 1 and plotted as Fig. 2 of [16]. Empirically, we find by comparing data from 16^3 , $16^2 \times 24$ and 24^3 lattices that the dominant correction on a $L_s^2 \times L_t$ system appears due to finite L_t , suggesting a specifically thermal origin. This motivates an extrapolation to the thermodynamic limit which is linear in $1/L_t$; at smaller j , however, the data depart significantly from this trend.

Assuming a $1/L_t$ scaling, we extrapolated the data from 24^3 and 32^3 lattices to estimate $\langle qq_+(j) \rangle$ in the thermodynamic limit. The results are shown on a log-log plot in Fig. 5, together with unextrapolated data from the chirally broken phase at $\mu = 0.0, 0.2$. Remarkably, there is a reasonably wide interval $j \in [0.05, 0.2]$ within which the plot is approximately linear, indicative of a power-law scaling

$$\langle qq_+(j) \rangle \propto j^\alpha. \quad (3.1)$$

Fits to (3.1) in this range yield $\alpha = 0.314(2)$ for $\mu = 0.8$, with $\chi^2/\text{dof} = 2.3$, and $\alpha = 0.213(3)$ for $\mu = 0.9$, with $\chi^2/\text{dof} = 0.4$. In both cases this is clearly distinct from the linear (ie. $\alpha = 1$) behaviour observed at low density. For j outside the fitted range, the data start to fall below the fitted line; we ascribe this to scaling violations for $j \gtrsim 0.25$, as perhaps revealed by the crossing of the curves in Fig. 3, and for $j \lesssim 0.035$ to non-thermal finite volume effects, eg. due to an insufficiently large explicit Majorana mass, as perhaps indicated by the different systematics of the 16^3 point in Fig. 4. Unfortunately our resources have not permitted further systematic study of this point.

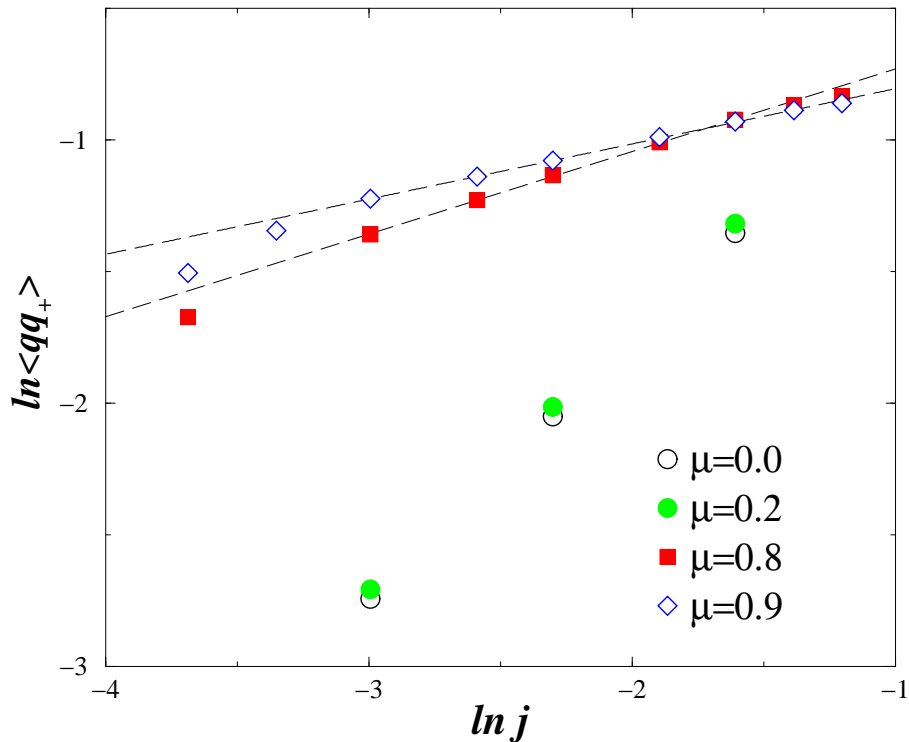


Figure 5: $\ln \langle qq_+ \rangle$ vs. $\ln j$, showing evidence for power-law scaling in the dense phase.

Assuming the validity of the form (3.1), we draw two conclusions. Firstly, the non-analytic behaviour is reminiscent of the power-law scaling observed at a critical point of a thermodynamic system. For a spin system at its critical temperature the spontaneous magnetisation \mathcal{M} scales with applied magnetic field h as $\mathcal{M} \propto h^{\frac{1}{\delta}}$ [28]; for a fermionic model exhibiting chiral symmetry breaking the equivalent relation is $\langle \bar{\psi}\psi \rangle \propto m^{\frac{1}{\delta}}$ [18]. We thus identify critical scaling, with $\delta \equiv \alpha^{-1}$. Secondly, Fig. 2 leads us to expect that critical behaviour is generic in the dense phase, but with the exponent δ varying continuously with chemical potential μ , taking the value $\delta \approx 3$ at $\mu = 0.8$ and ≈ 5 at $\mu = 0.9$. This suggests a line of critical points for $\mu > \mu_c$. The origins of such behaviour and its consequences for superfluidity will be elaborated in Sec. 4. In an attempt to find further evidence for criticality, however, we now switch attention from one- to two-point functions in a study of the various susceptibilities.

3.3 Susceptibilities

Next we examine the diquark susceptibilities χ_{\pm} defined by (2.12), which may be expanded to

$$\begin{aligned} \chi_{\pm} = \frac{1}{4} \sum_x & \langle \chi^{tr} \tau_2 \chi(0) \chi^{tr} \tau_2 \chi(x) + \bar{\chi} \tau_2 \bar{\chi}^{tr}(0) \bar{\chi} \tau_2 \bar{\chi}^{tr}(x) \rangle \\ & \pm \langle \chi^{tr} \tau_2 \chi(0) \bar{\chi} \tau_2 \bar{\chi}^{tr}(x) + \bar{\chi} \tau_2 \bar{\chi}^{tr}(0) \chi^{tr} \tau_2 \chi(x) \rangle. \end{aligned} \quad (3.2)$$

A generic susceptibility may be expressed as the sum of two connected contributions corresponding to the two possible Wick contractions,

$$\chi = \left[\langle (\text{tr} \Gamma \mathcal{G}_{xx})^2 \rangle - \langle \text{tr} \Gamma \mathcal{G}_{xx} \rangle^2 \right] + \langle \text{tr} \mathcal{G}_{0x} \Gamma \mathcal{G}_{0x}^{tr} \Gamma \rangle \equiv \chi^s + \chi^{ns}, \quad (3.3)$$

where $\mathcal{G} = \mathcal{A}^{-1}$ is the Gor'kov propagator and Γ projects out the appropriate components. By analogy with meson physics we label these contributions ‘‘singlet’’ and ‘‘non-singlet’’ respectively. Estimates for χ_{\pm}^s are made with the same stochastic method used for $\langle qq_+ \rangle$, and are plotted for $\mu = 0.8$ on a 32^3 lattice in Fig. 6. Apart from the observation that $\chi_-^s \approx \chi_+^s$, no other trend is apparent in the data, which are noisy and quite possibly consistent with zero. In the following we ignore χ_{\pm}^s and assume $\chi_{\pm} \simeq \chi_{\pm}^{ns}$. This is in marked contrast with the behaviour observed in studies of chiral symmetry breaking in $2+1d$ fermionic models, where singlet contributions to the relevant susceptibility are significant [29] or even dominant [10].

Restricting attention to the non-singlet pieces, it is not hard to show using the properties of \mathcal{G} reviewed in Sec. 5 below, that the first expectation value on the right hand side of (3.2) is negative and vanishes in the limit $j \rightarrow 0$, whereas the second is positive and in fact corresponds to the diquark correlator examined for $j = 0$ in [15]. We conclude that $|\chi_-| > |\chi_+|$. Data for χ_{\pm}^{ns} from a 32^3 lattice are shown in Fig. 7. Data at $\mu = 0.0$ are indistinguishable from those at $\mu = 0.2$ on the scale plotted. Note the difference of scale on the vertical axis between Figs. 6 and 7. We should also comment that the χ_-^{ns} data when checked against $\langle qq_+ \rangle$ saturate the Ward identity (2.13) within errors. Both observations justify our neglect of χ_{\pm}^s .

In a conventional symmetry breaking scenario χ_- should diverge in the thermodynamic and $j \rightarrow 0$ limits according to (2.13), whereas χ_+ could in principle remain finite. The ratio R defined in (2.14) is expected to vanish as $j \rightarrow 0$ if $U(1)_B$ symmetry is spontaneously broken by the ground state, and to approach unity if the symmetry remains manifest. In order to investigate this it is once again necessary to take account of finite volume effects. There is no appreciable effect for $\mu < \mu_c$, but in the

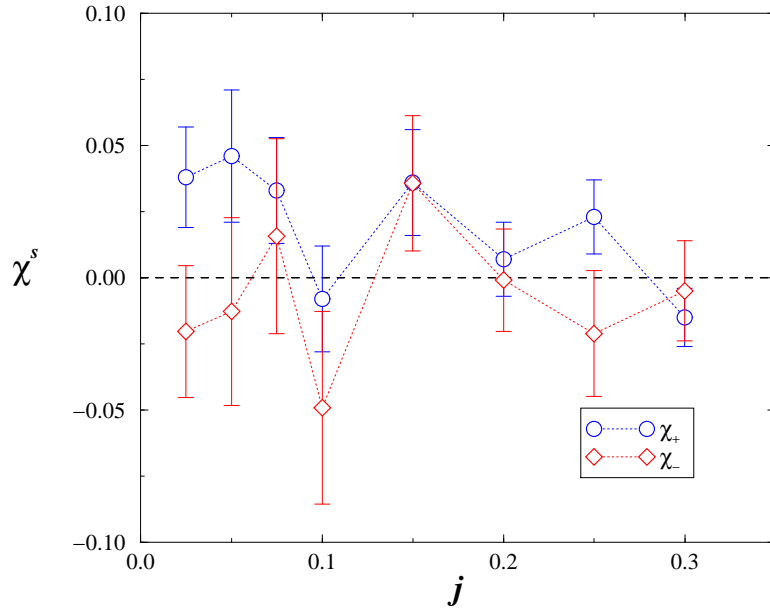


Figure 6: χ^s vs. j for $\mu = 0.8$ on a 32^3 lattice.

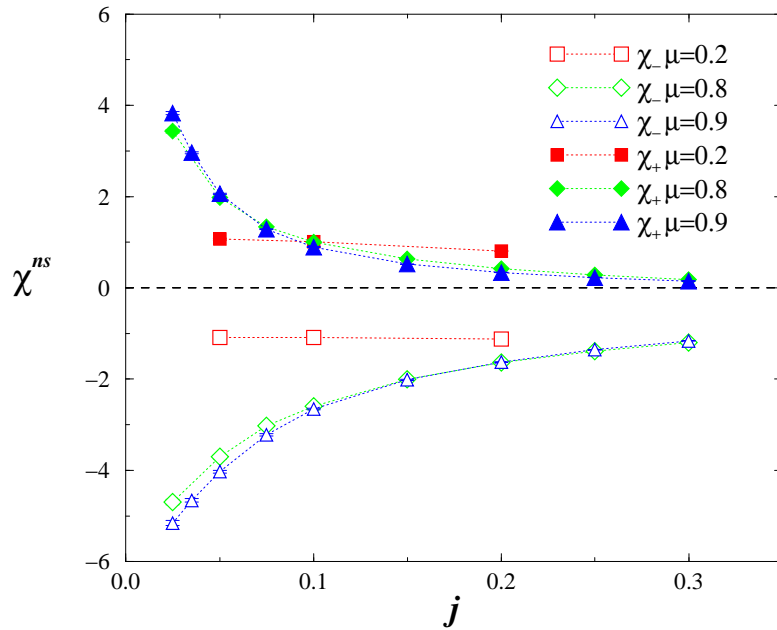


Figure 7: χ_+^{ns} (filled) and χ_-^{ns} (open) vs. j for various μ on a 32^3 lattice.

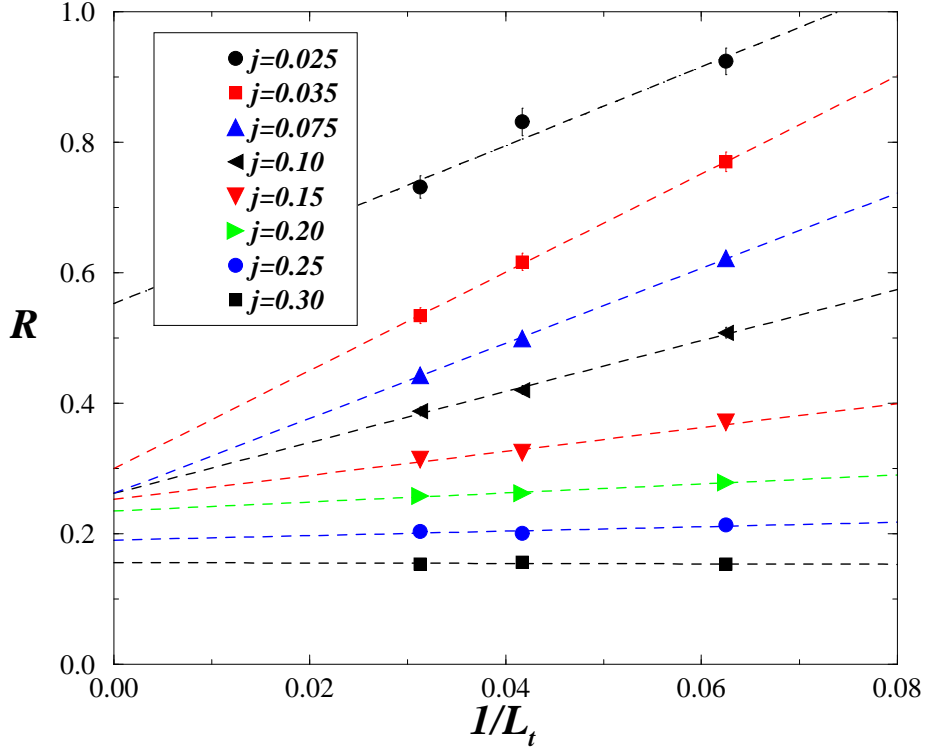


Figure 8: Susceptibility ratio R at $\mu = 0.8$ for various lattice sizes.

dense phase the variation with lattice size is considerable, as shown in Fig. 8. Once again, an extrapolation $\propto L_t^{-1}$ seems plausible, and indeed in this case a linear fit to the data from all three available volumes proved acceptable. The accumulation of the resulting intercepts in the region $R \simeq 0.3$ is striking.

The extrapolated results for R as a function of j are shown in Fig. 9. In the chirally broken phase the results support R tending smoothly to one as $j \rightarrow 0$, consistent with unbroken baryon number symmetry. The behaviour in the high-density phase is very different; the accumulation of intercepts in Fig. 8 manifests itself as a plateau for $j \gtrsim 0.075$. For smaller j the ratio shoots sharply upward towards one. This can be attributed to a finite volume artifact, since we know that terms in (3.2) of the form $\langle qq(0)qq(x) \rangle$ which split the degeneracy between χ_+ and χ_- necessarily vanish as $j \rightarrow 0$ away from the thermodynamic limit. In this regard it is encouraging that these non-thermal effects manifest themselves in the same range $j \lesssim 0.05$ observed for the condensate measurements of the previous section. We are thus motivated to attempt a linear extrapolation to $j = 0$ for the data with $j \in [0.75, 0.2]$. The fits are

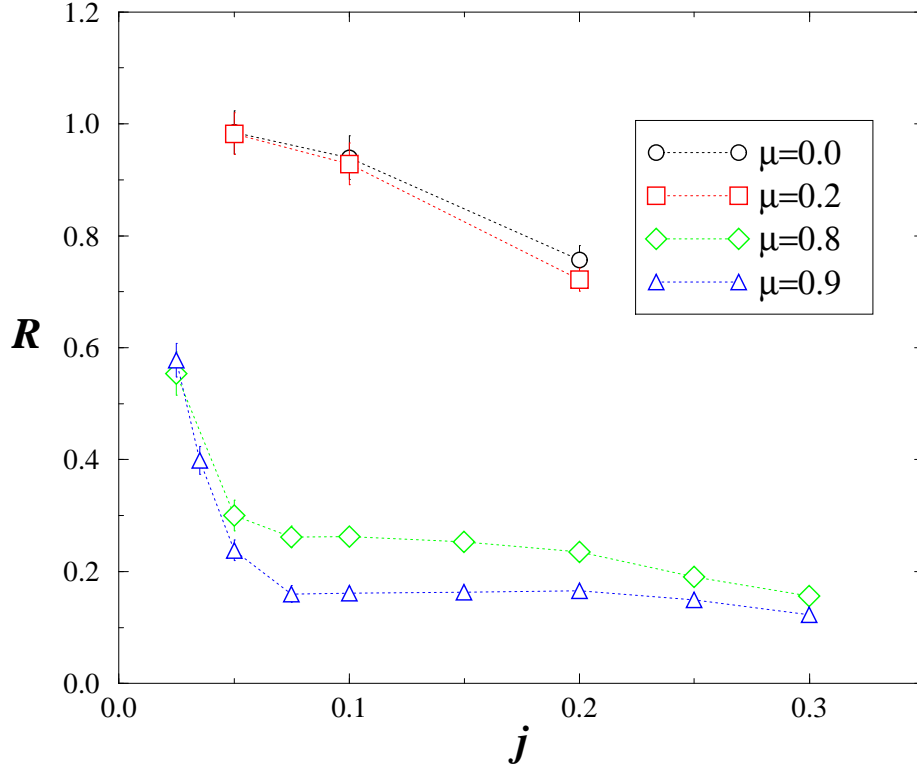


Figure 9: Susceptibility ratios R extrapolated to infinite volume for various $\mu = 0.8$.

of excellent quality and yield $R(j=0) = 0.29(2)$ for $\mu = 0.8$ and $R(j=0) = 0.17(1)$ for $\mu = 0.9$.

Measurements of the diquark condensate of Sec. 3.2 support a power-law form $\langle qq_+ \rangle \propto j^\alpha$ (3.1). If this is the case, then the relation $\chi_+ = \partial \langle qq_+ \rangle / \partial j_+$ together with the Ward identity (2.13) imply [30]

$$R(j) = \frac{\partial \ln \langle qq_+ \rangle}{\partial \ln j_+} = \alpha, \quad (3.4)$$

which crucially is independent of j . The plateaux of Fig. 9 clearly support this interpretation; moreover the values we obtain for $R(j=0)$ are in surprisingly good agreement with those from fits to (3.1). The susceptibility measurements thus provide an independent corroboration of the hypothesis that the system is critical for $\mu > \mu_c$.

3.4 Diquark Masses

Our final numerical study in this sector is of the spatial behaviour of the diquark correlation functions, in an attempt to estimate the masses M_{\pm} of diquark bound states. For brevity we only consider $\mu > \mu_c$, in which case M_{\pm} are probably best thought of as the energies required to excite a diquark pair above the ground state. We have restricted our attention to the zero-momentum timeslice correlator $C_{\pm}(t) = \sum_{\vec{x}} \langle qq_{\pm}(\vec{0}, 0) qq_{\pm}(\vec{x}, t) \rangle$, so that the excited state must consist of quarks with equal and opposite momentum \vec{k} . Recall that in the presence of a Fermi surface, only quarks with $k \simeq k_F$ can be excited; the measurements presented here are not sensitive to this restriction, although it will prove a decisive factor in the quasiparticle study of Sec. 5. As in the previous section, we ignore “singlet” diagrams in calculating C_{\pm} .

Fig. 10 shows the correlators for $j = 0.025$ and 0.25 at $\mu = 0.8$. By virtue of its definition, C_{\pm} is clearly symmetric under time-reversal, in contrast to the correlators studied in [15]. It is also clear, as expected, that $|C_{-}| > |C_{+}|$, and that the difference between them grows with j . Close inspection of Fig. 10 suggests that a standard simple-pole fit to $C_{\pm}(t)$ will not succeed unless a constant term is included; we have therefore attempted fits of the form [15]

$$C_{\pm}(t) = P_{\pm} \left(\exp(-M_{\pm}t) + \exp(-M_{\pm}(L_t - t)) \right) + Q_{\pm}. \quad (3.5)$$

The plateau height Q_{+} would by the cluster property be proportional to $|\langle qq_{+} \rangle|^2$ if the condensate formed; however, the analysis of [15] showed that at $j = 0$, Q_{+} does not display the required extensive scaling with two-dimensional spatial volume. There is no obvious theoretical interpretation for Q_{-} .

Fig. 11 shows $M_{\pm}(j)$ for $\mu = 0.8, 0.9$ resulting from fits of (3.5) to timeslices 5 - 26. In most cases the χ^2/dof was $\lesssim 2.0$ and in no case exceeded 6.0. M_{\pm} is found to increase almost linearly with j , maintaining a roughly constant difference $M_{+} - M_{-} \simeq 0.08$ for $j \geq 0.05$. For smaller j the curvature in the plots suggests the two states may become degenerate as $j \rightarrow 0$. A linear extrapolation to $j = 0$ yields $M_{+}(\mu = 0.8) \simeq 0.23$, $M_{+}(\mu = 0.9) \simeq 0.21$, values of the same order of magnitude but slightly lower than those obtained directly at $j = 0$ on a $16^2 \times 24$ lattice in [15] (note that the symbols M_{\pm} have a different meaning in that paper). The fitted values for Q_{\pm} vary considerably over the range of j explored: eg. for $\mu = 0.8$, Q_{+} rises from $0.102(1) \times 10^{-5}$ at $j = 0.25$ to $0.315(5) \times 10^{-1}$ at $j = 0.025$; in the same range Q_{-} rises even more dramatically from $0.49(6) \times 10^{-7}$ to $0.279(7) \times 10^{-1}$.

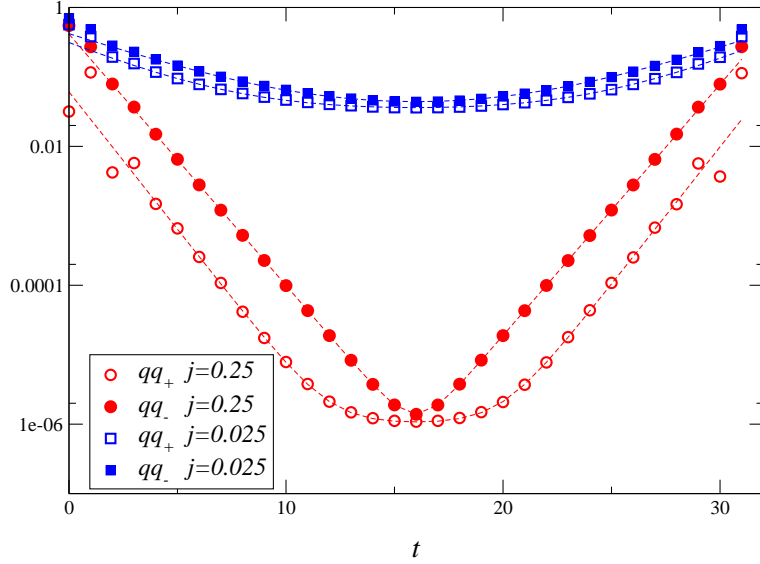


Figure 10: Diquark timeslice correlators $|C_{\pm}(t)|$ for two values of j at $\mu = 0.8$ on a 32^3 lattice.

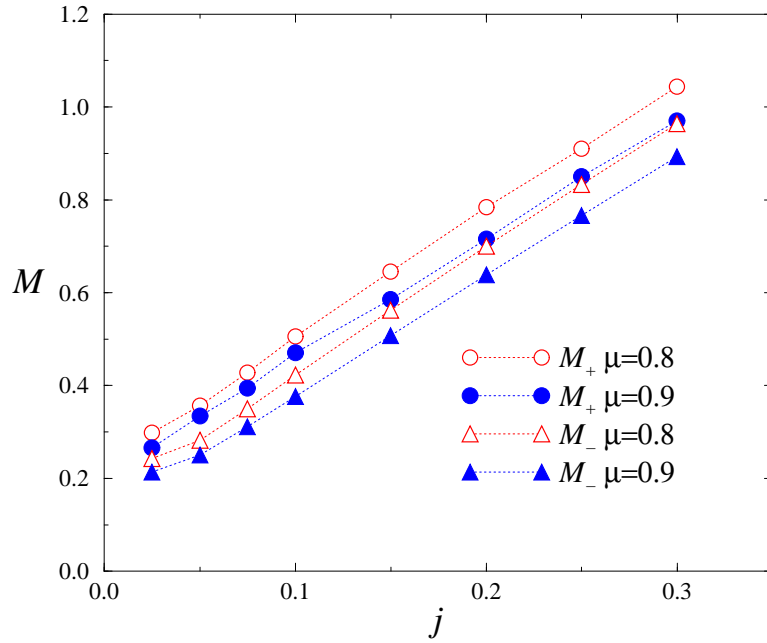


Figure 11: Diquark masses extracted from fits to (3.5) on a 32^3 lattice.

The most important feature of Fig. 11 is that there is no evidence for M_- vanishing as $j \rightarrow 0$, as might be expected if qq_- coupled to a Goldstone mode as a result of broken $U(1)_B$ symmetry. One might argue that the *ad hoc* inclusion of Q_- in the fit (3.5) results in artificially high values of M_- ; in any case, the conclusion remains that simple pole fits to $C_-(t)$ corresponding to a weakly interacting Goldstone boson in this channel fail drastically. The scaling form (3.1) combined with the Ward identity (2.13) implies a massless degree of freedom as $j \rightarrow 0$, and hence long range correlations, in both qq_- and (since symmetry is restored in this limit) qq_+ channels; they must, however, be strongly interacting and hence short-lived states.

4 Criticality and Superfluidity

Having established that in the limit of vanishing source there is no diquark condensation at high density, but instead a critical phase with the scaling of the condensate with the source governed by an exponent δ varying continuously with μ , we now discuss the implications for possible superfluid behaviour of the $2+1d$ NJL model. In fact, this result is in accordance with well-known theorems that long range ordering of a two-dimensional system with a continuous global symmetry is impossible [31]. In the current context a particularly appropriate statement of the theorem is due to Hohenberg [32], who explicitly considers the case of a composite order parameter via Cooper pairing in a low-dimensional fermion superfluid. Long-wavelength fluctuations of the phase θ of the would-be condensate always wash out the order in the zero source limit. In field theoretic language, in two dimensions infra-red divergences dictate that the Goldstone pole in the transverse susceptibility predicted by a naive application of (2.13) is replaced by a softer divergence consistent with a power-law decay of the correlator

$$\lim_{j \rightarrow 0} \langle qq_-(0)qq_-(r) \rangle \propto \langle e^{i\theta(0)} e^{-i\theta(r)} \rangle \propto \frac{1}{r^\eta}, \quad (4.1)$$

where η is another critical exponent, implying a massless but strongly-interacting mode and long-ranged phase correlations. Note that direct numerical tests of (4.1) would require data from spatial diquark correlators, in contrast to the temporal correlators explored in Sec. 3.4. There are also technical difficulties in taking the limit $j \rightarrow 0$.

The best known example of a system with a critical phase is the $2d$ O(2) spin or XY model, which is similar in that long range order would also spontaneously

break a U(1) global symmetry. The critical behaviour occurs for $T < T_{BKT}$, the temperature of the celebrated Berezinskii-Kosterlitz-Thouless transition [20, 33]. The physical picture can be explained as follows; on the assumption that the interaction strength is a periodic function of the difference in angle θ between adjacent spins, and is approximately gaussian in neighbourhood of its minima, then an effective Hamiltonian can be written as

$$H_{XY}[\theta, m] = J \sum_{x\mu} (\partial_\mu \theta(x))^2 - 2\pi J \sum_{\tilde{x}, \tilde{y}} m(\tilde{x}) \ln \left| \frac{\tilde{x} - \tilde{y}}{r_0} \right| m(\tilde{y}), \quad (4.2)$$

J being the nearest neighbour coupling. In addition to the θ s the Hamiltonian depends on integer-charged *vortices* $m(\tilde{x})$ located on the sites of the dual lattice. The vortices are topological excitations of the spins which interact via a Coulomb potential which is logarithmic in two dimensions, ensuring that all configurations with finite H_{XY} are overall charge-neutral, ie. contain as many anti-vortices as vortices. The parameter r_0 is the ‘‘core size’’ of the vortex, which can be considered of the same order as the lattice spacing. Now, at low temperatures the second term of (4.2) strongly suppresses well-separated vortex – anti-vortex pairs, and the model’s dynamics are dominated by small-amplitude fluctuations of θ , the so-called *spin waves*. Phase correlations are governed by (4.1) with $\eta(T) = T/4\pi J$, implying a critical phase with continuously varying exponent. At the critical temperature T_{BKT} , the vortex entropy begins to dominate the free energy of the system, and vortex pairs of arbitrary separation form. The resulting vortex plasma screens long range correlations resulting in a finite correlation length for $T > T_{BKT}$.

Next we discuss the relation with superfluidity. We can rewrite the diquark operator $qq_+(x) = \phi(x) = \phi_0 e^{i\theta(x)}$, where the constant ϕ_0 is the density of quark pairs participating in the condensate and θ the local phase of the diquark operator. In this form $qq_+(x)$ can be regarded as a bosonic *macroscopic wavefunction* for the condensed pairs. We now identify a superfluid current $J_{s\mu}$ via

$$J_{s\mu} \propto -\frac{i}{2} (\phi^* \partial_\mu \phi - (\partial_\mu \phi^*) \phi) = K_s \partial_\mu \theta. \quad (4.3)$$

The constant K_s must be determined empirically. In the non-relativistic limit it is given by

$$K_s = \frac{\hbar}{M} n_s \quad (4.4)$$

where M is the mass of the current-carrying atomic species ($M(^4\text{He})$ or $2M(^3\text{He})$ in the case of the two known superfluids), and n_s a parameter called the *superfluid*

density, which for an interacting system need not coincide with the charge density of the particles in the condensate [22]. In turn this enables the definition of a *superfluid velocity* $\vec{v}_s = \frac{\hbar}{M} \vec{\nabla} \theta$. For a relativistic system the relation $\vec{v}_s = \frac{\hbar}{2\mu} \vec{\nabla} \theta$ can be shown to hold for diquark pairs for small v_s [34].

Now in the static limit, relation (4.3) implies that the flow is irrotational, viz. $\vec{\nabla} \times \vec{J}_s = \vec{0}$, and hence the circulation $\kappa = \oint \vec{J}_s \cdot d\vec{l}$ around any closed path vanishes unless either the condensate is somewhere singular within the contour, ie. $\phi_0 = 0$, or the space is non-simply connected. In either case the requirement that θ be single-valued results in the quantisation of circulation: $\kappa = 2\pi n K_s$, with n integer. In the case of a singularity in ϕ the physical realisation of $\kappa \neq 0$ is a vortex, with a non-zero radius r_0 within which the normal phase is restored. Superfluid vortices experience long-ranged mutual interactions; for a two-dimensional system such vortices can be identified with the vortices of the XY model, and are expected to be governed by an effective Hamiltonian of the same form as (4.2). An example of a non-simply connected space would be a finite system of dimension $L_x \times L_y$ with periodic boundary conditions; in this case $\kappa \neq 0$ implies a uniform supercurrent

$$\vec{J}_s(n_x, n_y) = 2\pi K_s \left(\frac{n_x}{L_x} \hat{x} + \frac{n_y}{L_y} \hat{y} \right). \quad (4.5)$$

The crucial point is that the resulting flow patterns are topologically stable, implying the system's energy must be greatly increased to change κ [20]. For instance, in order to change n_x by one unit, a vortex – anti-vortex pair must be created and the vortex moved in the y -direction right around the system before being allowed to reannihilate with the anti-vortex. In so doing the system must be brought through a saddle-point configuration in which the pair is separated by half the system extent; from (4.2) the energy required $\sim 2\pi J \ln(L_y/2r_0)$. Since this diverges with the size of the system, we infer that the circulation is stable and hence the current \vec{J}_s persistent, implying superfluidity. We conclude that the critical phase of the XY model, and by extension critical behaviour in any two dimensional system with a U(1) global symmetry, describes superfluidity despite the absence of a condensate. Long range order of the phase θ is not necessary; phase coherence, as expressed by (4.1), is sufficient. It is noteworthy in this regard that some of the most precise tests of the universal predictions of the XY model have come from studies of thin films of superfluid ^4He [19].

Since we have used universal features of vortices and spin waves to argue that critical behaviour implies superfluidity in two dimensions, to justify the application

of these ideas to the NJL model we should address the issue of why our δ is not consistent with that of the XY model as revealed by a renormalisation group analysis [35], which predicts

$$\delta \geq 15 \quad ; \quad \eta \leq \frac{1}{4}, \quad (4.6)$$

with equality holding as $T \rightarrow T_{BKT-}$. First we note that dimensional reduction, which predicts that the critical thermal properties of $2+1d$ systems should be governed by the $2d$ spin model with equivalent global symmetry, does *not* apply in this case (see [36] for a recent numerical study of a four-fermi model with $U(1)$ axial symmetry at $T \neq 0$ which does appear consistent with the BKT scenario). Rather, the feature which permits us to use a two-dimensional effective model is the static nature of the phase fluctuations, ie. $\partial_t \theta \simeq 0$, as evidenced by the plateaux observed in the large- t behaviour of diquark correlation functions in [15] and Sec. 3.4. Note in addition that we have needed the limit $L_t \rightarrow \infty$ rather than $L_t \rightarrow 0$. Since the number of accessible Matsubara modes in our simulations remains large, the fermions need not decouple (indeed, there remain light fermionic excitations, as we shall see in Sec. 5) and we should not expect the model's dynamics to be described by a purely bosonic effective action. Symmetry breaking via a composite order parameter is qualitatively different from cases where the order parameter is an elementary field; there is a wealth of evidence, both analytical and numerical, that bosonic and fermionic models with the same patterns of global symmetry breaking belong to separate universality classes in dimensions up to [17, 18, 29, 37] and even including [23] four.

Our simulations have yielded information only about the critical exponent δ in the dense NJL model. Our results $\delta(\mu = 0.8) \approx 3$, $\delta(\mu = 0.9) \approx 5$ are consistent with a critical phase for $\mu > \mu_c$. The lower numerical values as compared to (4.6) typify the distinct nature of symmetry breaking via a composite order parameter as discussed above. Note, however, that although δ decreases with μ , the analogous μ_{BKT} at which superfluid vortices unbind may not be physically accessible; most probably chiral symmetry breaking at $\mu = \mu_c$ happens first. Finally, although we have not yet found a method to measure η , it is interesting to estimate its value using the hyperscaling relation $\delta = (d + 2 - \eta)/(d - 2 + \eta)$ [28]. Since we have assumed an effective dimension $d = 2$ for the critical dynamics, the appropriate relation is

$$\delta = \frac{4 - \eta}{\eta}, \quad (4.7)$$

yielding $\eta(\mu = 0.8) \approx 1$ and $\eta(\mu = 0.9) \approx 0.7$. Note that had we used an effective dimension $d = 3$, the prediction for η at $\mu = 0.9$ would be almost vanishing.

5 The Quasiparticle Spectrum

In this section we study the spin- $\frac{1}{2}$ sector by examining the Gor'kov propagator $\mathcal{G} = \mathcal{A}^{-1}$ as a function of μ and j . For $\mu < \mu_c$ the fermion excitations are simply related to those at $\mu = 0$, as reported in [11]. For $\mu > \mu_c$, however, the ground state of the model changes radically, and is characterised by a Fermi surface with energy E_F and characteristic momentum k_F . A generic description is Fermi liquid theory [21, 22], in which excitations with momentum k such that $|k - k_F| \ll k_F$ are quasiparticles whose mass need not coincide with that of the fundamental quanta. If a BCS condensation occurs, then the lowest energy excitation may be separated from zero by a gap Δ , and the quasiparticles may not be eigenstates of baryon number, but instead some kind of particle-hole superposition. Analysis of \mathcal{G} using standard lattice spectroscopy techniques yields information on the quasiparticle dispersion relation $E(k)$, thus probing Δ and, more generally, the nature of the model's Fermi surface.

We begin by making some general observations about the Gor'kov propagator. Write

$$\mathcal{G}(x, y) = \begin{pmatrix} A(x, y) & N(x, y) \\ \bar{N}(x, y) & \bar{A}(x, y) \end{pmatrix}, \quad (5.1)$$

where each element denotes a 2×2 matrix in isospace. Our notation signifies that the propagator contains both “normal” $\langle q(x)\bar{q}(y) \rangle$ and “anomalous” $\langle q(x)q(y) \rangle$ components, together with their barred counterparts. On a finite system, A and \bar{A} vanish in the limit $j \rightarrow 0$, and N, \bar{N} become proportional to the usual fermion and anti-fermion propagators. The number of independent components of \mathcal{G} is constrained by certain identities. For instance, N is proportional to an element of $SU(2)$, implying $N_{22} \equiv N_{11}^*$ and $N_{21} \equiv -N_{12}^*$, with similar relations for \bar{N} . In the anomalous sector, however, it is $\tau_2 A$ which resembles an $SU(2)$ matrix so the equivalent identities are $A_{22} \equiv -A_{11}^*$ and $A_{21} \equiv A_{12}^*$. These relations imply that a column of \mathcal{G} can be reconstructed using just two conjugate gradient inversions of $\mathcal{A}[\Phi]$.

We first examined the timeslice propagator $\mathcal{G}(t) = \sum_{\vec{x}} \mathcal{G}(\vec{0}, 0; \vec{x}, t)$ and empirically found the following features:

- For $t \neq 0$, $\text{Re}\langle N_{11}(t) \rangle \approx \text{Re}\langle \bar{N}_{11}(L_t - t) \rangle$, ie. the antifermion propagator is related to that of the fermion by time reversal.
- $\text{Im}\langle N_{11} \rangle \approx \text{Im}\langle \bar{N}_{11} \rangle \approx \langle N_{12} \rangle \approx \langle \bar{N}_{12} \rangle \approx 0$: the vanishing of the off-diagonal components of N is consistent with isopin $SU(2)_V$ symmetry.

- $\text{Im}\langle A_{12}(t) \rangle \approx \text{Im}\langle \bar{A}_{12}(t) \rangle \approx -\text{Im}\langle A_{12}(L_t - t) \rangle$, ie. in the anomalous sector fermion and antifermion have equivalent behaviour under time-reversal.
- $\text{Re}\langle A_{12} \rangle \approx \langle A_{11} \rangle \approx \langle \bar{A}_{11} \rangle \approx 0$, ie. isopin symmetry in the anomalous sector demands the diagonal components vanish.

From here on for convenience we will denote $\text{Re}N_{11}$ by N and $\text{Im}A_{12}$ by A . In Fig. 12 we plot $\ln |N(t)|$ vs. t for two values of μ in the low density chirally broken phase. At $\mu = 0$ the propagator is symmetric under time reversal, and the fermion mass $\Sigma \simeq 0.730(2)$, consistent with the breaking of chiral symmetry. At $\mu = 0.2$ the time-reversal symmetry is broken; one state propagates forwards with mass $0.952(4)$, the other backwards with mass $0.530(2)$, corresponding approximately to masses $\Sigma \pm \mu$. Now, since $n_B = 0$ for $\mu < \mu_c$, the ground state is unchanged and the physical interpretation of this result is simply that the chemical potential shifts the energies required to excite fermions and anti-fermions in opposite directions, the anti-fermion travelling in the $+t$ direction and the particle $-t$.

For $\mu > \mu_c$ the situation is completely altered. Recall that in the presence of a Fermi surface excitations have a characteristic momentum scale k_F . Therefore it is necessary to introduce momentum dependence into the Gor'kov propagator via $\mathcal{G}(\vec{k}, t) = \sum_{\vec{x}} \mathcal{G}(\vec{0}, 0; \vec{x}, t) e^{-i\vec{k}\cdot\vec{x}}$ [16]. We choose \vec{k} oriented along a lattice axis, and the set \vec{x} to include only sites an even number of lattice spacings from the origin in each direction, so that the physically accessible momenta are given by $k = \frac{2\pi n}{L_s}$ with $n = 0, 1, \dots, L_s/4$. Fig. 13 shows both normal and anomalous propagators in the high density phase for $k = \frac{\pi}{4}$. Note that now $N(t) \approx 0$ for t even, and $A(t) \approx 0$ for t odd. This is a manifestation of the restored $\text{SU}(2)_L \otimes \text{SU}(2)_R$ symmetry (2.5), which would be broken by any $N_{ee,oo}$ or $A_{oe,eo} \neq 0$. We have found that the propagators for various j and k are well fitted on every second timeslice by the following forms, with fit parameters A, B, C and E :

$$N(k, t) = Ae^{-Et} + Be^{-E(L_t-t)}, \quad (5.2)$$

$$A(k, t) = C(e^{-Et} - e^{-E(L_t-t)}). \quad (5.3)$$

The resulting $E(k, j)$ is the quasiparticle *dispersion relation*. We have studied this function in detail on a 32^3 lattice, which has 9 distinct values of k , performing fits to (5.2) over the range $t \in [5, 27]$. The fits are of excellent quality, with χ^2/dof rarely exceeding 2.0. We are naturally interested in the $\text{U}(1)_B$ symmetric limit; Fig. 14 shows that $E(k, j)$ can be smoothly extrapolated to $j = 0$, and we quote the

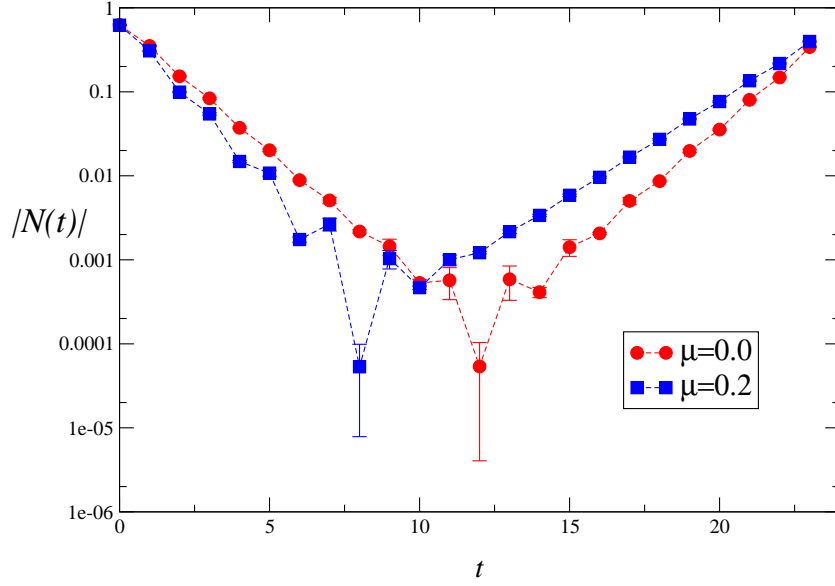


Figure 12: Normal propagators $|N(t)|$ for $\mu = 0.0$ and $\mu = 0.2$ on a $16^2 \times 24$ lattice with $j = 0.1$.

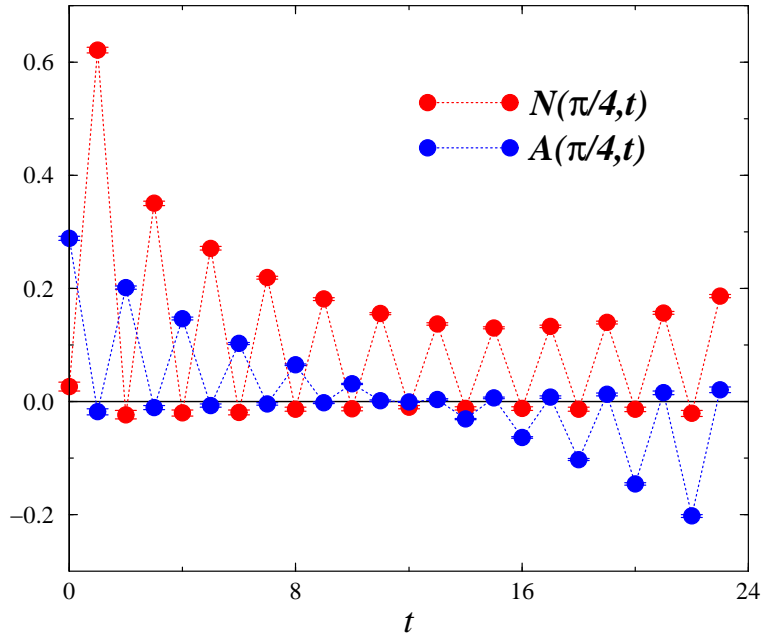


Figure 13: Normal and anomalous propagators with $k = \frac{\pi}{4}$ at $\mu = 0.8$ on a $16^2 \times 24$ lattice with $j = 0.1$.

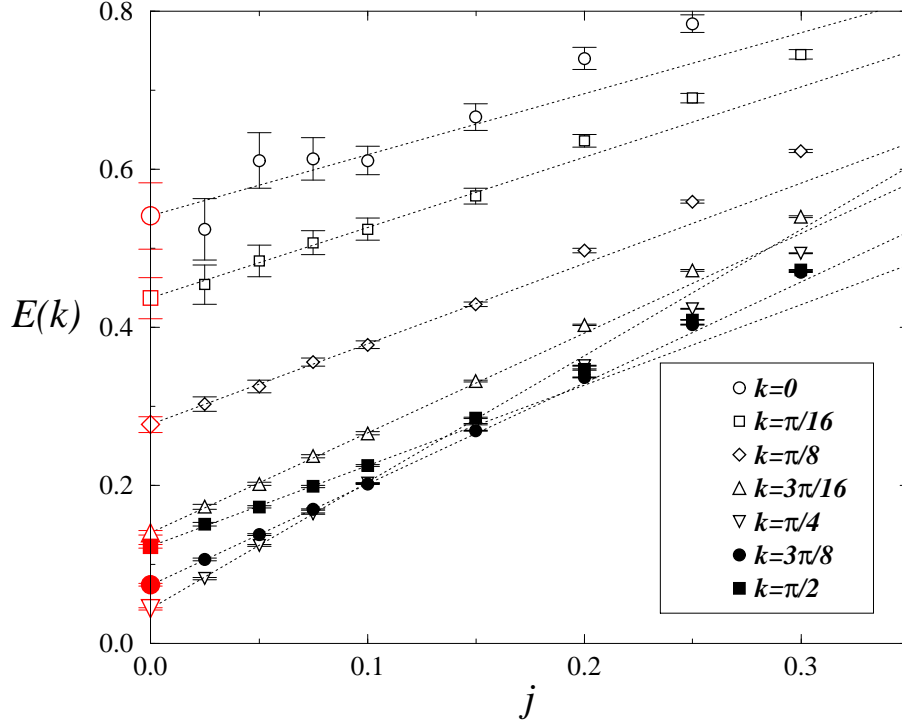


Figure 14: $E(k, j)$ vs. j extracted from fits to (5.2) on a 32^3 lattice with $\mu = 0.8$. Open symbols denote excitations on the hole branch, and closed symbols the particle branch.

results of linearly extrapolating the data with $j \in [0.025, 0.1]$. Fits to the anomalous propagator $A(k, t)$ yield quantitatively very similar results for $E(k, j)$.

The caption of Fig. 14 assigns different k ranges to a “hole branch” (E decreases with k) and a “particle branch” (E increases with k). It is straightforward to verify this interpretation by considering the free Euclidean propagator $S_F(k) = (i\vec{k} + \mu\gamma_0 + m)^{-1}$. For fixed spatial momentum, with $\mu < E(k) = \sqrt{\vec{k}^2 + m^2}$,

$$S_F(\vec{k}, t) = \begin{cases} \frac{m}{2E}(1 + \mathcal{V}^-)e^{-(E+\mu)t} & t > 0; \\ \frac{m}{2E}(1 - \mathcal{V}^+)e^{-(E-\mu)|t|} & t < 0, \end{cases} \quad (5.4)$$

where the complex “4-velocity” $V_\mu^\pm \equiv (E, \pm i\vec{k})/m$. The propagator has both forwards and backwards-decaying signals, each associated with a different projection operator; in the limit $\vec{k} \rightarrow \vec{0}$ these become $\frac{1}{2}(1 \pm \gamma_0)$ and thus project onto anti-fermion and fermion states respectively. The fermion, being lighter, dominates the signal for $\mu t \gg 1$ yielding a predominantly backward propagation. For $\mu > E(k)$, however,

there is only a forwards-moving signal, once again dominated by the fermion:

$$S_F(\vec{k}, t) = \frac{m}{2E} \Theta(t) \left[(1 + \mathcal{V}^-) e^{-(\mu+E)t} - (1 - \mathcal{V}^+) e^{-(\mu-E)t} \right]. \quad (5.5)$$

For free fermions the transition between (5.4) and (5.5) takes place at a sharply defined Fermi energy $E_F = \sqrt{k_F^2 + m^2} = \mu$. Excitations with $k > k_F$, the Fermi momentum, add particles to levels above the Fermi surface; those with $k < k_F$ vacate holes in the Fermi Sea. The energy cost is smallest when $k \simeq k_F$.

In Fig. 15 we plot the amplitudes A, B and C from the fits to (5.2,5.3) and confirm that for small k , $N(k, t)$ is dominated by a forwards-moving signal, but there is a rather sharp crossover to backwards propagation at $k/\pi \simeq 0.3$. This transition becomes sharper as $j \rightarrow 0$; however, we plot data with $j \neq 0$ to show that the amplitude C only differs significantly from zero for momentum states in the neighbourhood of the Fermi surface. Were a BCS gap to form, we would expect $\lim_{j \rightarrow 0} C(j) \neq 0$ indicating particle-hole mixing; our data, however, do not give strong support for this.

Fig. 16 shows the dispersion relation $E(k)$ extrapolated to $j = 0$ for $\mu = 0.8$, together with points derived from the free Gor'kov propagator (ie. generated with $g^2 = 0$) using the identical procedure. We have plotted energies from the hole branch as negative in order to generate a smooth curve. There is no sign of any discontinuity characteristic of a BCS gap $\Delta \neq 0$. In order to interpret the detailed form of the curve it is necessary to take account of discretisation effects; for free massless fermions the expected dispersion relation, shown as a solid curve in Fig. 16 is $E(k) = -\mu + \sinh^{-1}(\sin k)$. We have found that a reasonable fit to our data for $\mu \in [0.8, 0.9]$, shown as a dashed line in Fig. 16, is given by

$$E(k) = -E_0 + D \sinh^{-1}(\sin k). \quad (5.6)$$

Eqn. (5.6) predicts a sharply defined effective Fermi momentum given by

$$K_F \equiv \sinh^{-1}(\sin k_F) = E_0/D. \quad (5.7)$$

In addition it is possible to define a quasiparticle group velocity $\beta = \partial \sinh(E + E_0) / \partial \sin k$, whose value

$$\beta_F = D \frac{\cosh E_0}{\cosh K_F} \quad (5.8)$$

at the Fermi surface is the *Fermi velocity*, which helps to characterise the Fermi liquid. For free massless fermions $K_F = \mu$ and $\beta_F = 1$ for all μ . Our fitted values of K_F and β_F are given in Table 2.

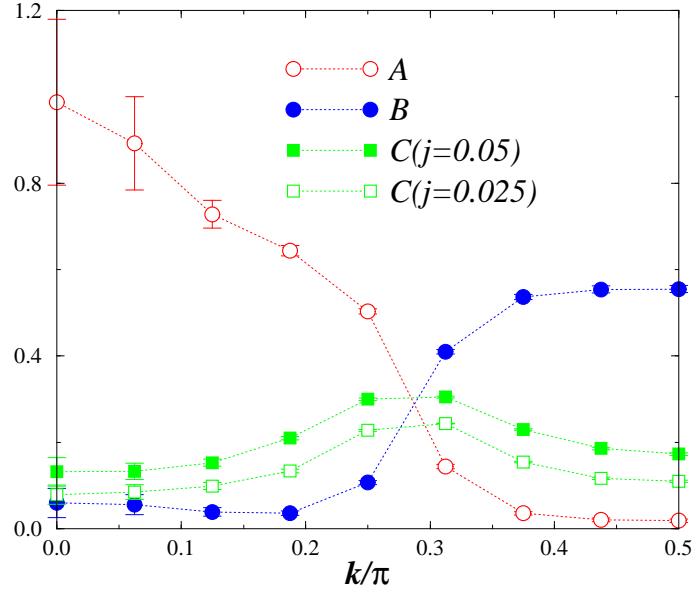


Figure 15: The amplitudes A, B and C extracted from fits to (5.2,5.3) on a 32^3 lattice with $\mu = 0.8$. The data for A and B were taken with $j = 0.025$.

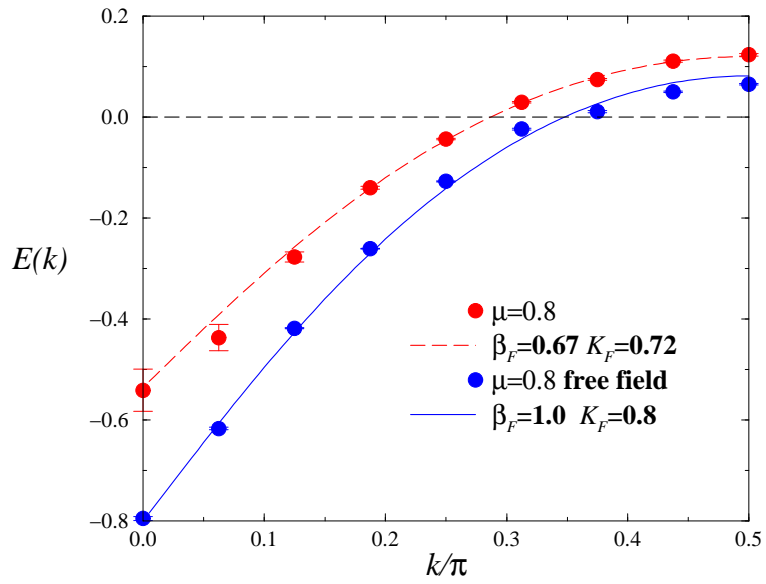


Figure 16: Dispersion relation $E(k)$ at $\mu = 0.8$ on a 32^3 lattice for both interacting and free fermions.

Table 2: Quasiparticle parameters resulting from fits of (5.6) to data from a 32^3 lattice. The quoted errors are purely statistical.

μ	K_F	β_F	$K_F/\mu\beta_F$
0.80	0.720(3)	0.670(3)	1.34(1)
0.82	0.738(3)	0.671(3)	1.34(1)
0.84	0.773(3)	0.686(3)	1.34(1)
0.86	0.791(5)	0.673(4)	1.37(1)
0.88	0.811(5)	0.628(4)	1.47(1)
0.90	0.836(4)	0.704(4)	1.32(1)

Although the errors quoted in Table 2 are almost certainly underestimated, some systematic features are apparent. The observed values of K_F increase smoothly with μ , and are $\approx 90\%$ of their free-field values. The Fermi velocity β_F , by contrast, is more or less independent of μ , and only $\approx 70\%$ of the free-field value; ie. the quasiparticles travel at less than the speed of light. In non-relativistic Fermi liquid theory [21, 22], the ratio K_F/β_F defines a quantity called the *effective mass* M^* , which need not coincide with the mass of the fundamental atomic species M ; eg. for the archetypal Fermi liquid ${}^3\text{He}$ in the sub-kelvin (but non-superfluid) regime, $M^* \simeq 3M$ [22]. In Landau's theory the ratio for a two-dimensional fluid is given in terms of the dipole component of the interaction between quasiparticles, ie.

$$\frac{M^*}{M} = 1 + N_F \int_0^{2\pi} \frac{d\vartheta}{2\pi} f(\vartheta) \cos \vartheta, \quad (5.9)$$

where $N_F = gV_2 \frac{k_F}{2\pi\beta_F}$ is the number of quasiparticle states on the Fermi surface per unit energy interval (V_2 is the volume of $2d$ space and g counts independent spin and isospin components) and $f(\vartheta)$ the spin-singlet interaction energy between quasiparticles at the Fermi surface with momenta separated by angle ϑ . In a relativistic generalisation the left hand side of (5.9) is replaced by $K_F/\mu\beta_F$ [38]; we infer from the data of Table 2 that $\overline{f(\vartheta) \cos \vartheta} > 0$ when averaged over the Fermi circle, and the interaction hence repulsive between quasiparticles with parallel momenta and/or attractive if the momenta are anti-parallel (the simpler conclusion that the interaction is always attractive was wrongly drawn in [16]). This should be contrasted with the interaction between the fundamental fermions of the NJL model due to σ exchange, which is attractive and independent of direction¹. A similar effective reversal of sign arises in the Hartree-Fock treatment of free electron states in a metal [13], and is

¹Single π exchange is attractive in isosinglet but repulsive in isotriplet channels; the net binding effect in matter made from equal numbers of u and d quarks vanishes.

characteristic of a quantum-mechanical exchange effect.

To summarise, we have examined the quasiparticle spectrum and estimated both Fermi momentum K_F and velocity β_F with due allowance made for discretisation artifacts. The results are consistent with a relativistic generalisation of a Landau Fermi liquid, and qualitatively similar to the normal phase of liquid ${}^3\text{He}$. There is no evidence for a BCS gap, and in the $j \rightarrow 0$ limit the anomalous components of the propagator signalling particle-hole mixing probably vanish. We note, however, that superfluid behaviour is not precluded by the absence of a gap [22]; the unlimited growth of quasiparticle excitations that couple normal and superfluid components and hence destroy superfluidity in a gapless Bose liquid are here prevented by the Pauli Exclusion Principle. Long range phase coherence is a sufficient condition for superfluidity.

6 Summary and Outlook

Let us briefly review the main achievements of the paper. Firstly, we have developed the necessary formalism to identify diquark condensation in numerical lattice studies of field theories on finite systems at non-zero chemical potential, the crucial ingredient being the introduction of a diquark source term. Secondly, to our initial surprise, we have found no evidence for a condensate $\langle qq \rangle \neq 0$ in studies of the $2+1d$ NJL model in its high density phase $\mu > \mu_c$. Rather, the results from two independent analyses of diquark observables are consistent with a critical behaviour $\langle qq(j) \rangle \propto j^\alpha$ throughout the dense phase. Whilst there is some residual uncertainty about the source of finite volume effects for $j \lesssim 0.05$, we suspect it would require computer resources considerably greater than those we have used to modify this conclusion. Critical behaviour in two dimensions implies long range coherence in the phase of the condensate wavefunction, which is a sufficient condition for superfluidity. Whilst there is qualitative similarity with the well-known example of the low temperature phase of the $2d$ XY model, the measured value of the critical exponent δ is distinct, suggesting that the $2+1d$ dense NJL model belongs to a new universality class. Thirdly, we have performed the first systematic spectroscopic study in the spin- $\frac{1}{2}$ sector for $\mu \neq 0$, and mapped out the quasiparticle dispersion relation. The success of the simple pole fits (5.2, 5.3) confirms the long-lived nature of the quasiparticles. There is no evidence for either particle-hole mixing or $\Delta \neq 0$ in the $j \rightarrow 0$ limit. Instead, the system resembles a normal Fermi liquid with a well-defined Fermi surface; the Fermi velocity β_F is of

the same order as but significantly less than the free-field value 1. Our findings can be summarised by the statement that the high density phase of the 2+1d NJL model is a relativistic gapless thin film BCS superfluid.

In a sense this and related papers with $\mu \neq 0$ represent the primitive beginnings of the study of condensed matter physics on the lattice. Let us sketch a few possible future directions. Firstly, it would be interesting to estimate the supercurrent \vec{J}_s corresponding to a quantised flow pattern around a finite system as in (4.5), which could be set up using a spatially varying $j(x)$. As well as providing a direct demonstration of superfluidity, this would also enable the extraction of the phenomenologically important parameter K_s . Secondly, it is possible to study quasiparticles and other Fermi surface-related phenomena. For instance, a sharp Fermi surface leads to oscillations of spatial frequency $2k_F$ in the screened potential between static charges, known as Friedel oscillations [13, 39]. Friedel oscillations can be observed in the wavefunctions of $q\bar{q}$ and qq states in 2+1d four-fermi models with $\mu > \mu_c$ [40]. Another possibility is the observation of light $q\bar{q}$ mesons in the spin-1 channel, corresponding to low-energy excitations of the Fermi surface related to the phenomenon of zero sound [21, 22, 41]. Finally, it is of prime importance to extend our calculations to the physically relevant case of 3+1d. In this case the NJL model is no longer a fundamental field theory, but instead can be thought of as an effective description of strong interaction physics with many possible phenomenological applications including thermodynamics [42]. If our arguments are correct, then the “conventional” signals for a BCS mechanism, namely $\langle qq \rangle \neq 0$ and $\Delta \neq 0$ should be readily observed using the methods we have developed.

Acknowledgements

This work is supported by the TMR network “Finite temperature phase transitions in particle physics” EU contract ERBFMRX-CT97-0122. SJH also received support from the Leverhulme Trust.

References

- [1] J. Bardeen, L.N. Cooper and J.R. Schrieffer, Phys. Rev. **108** (1957) 1175.
- [2] L.P. Gor’kov, Sov. Phys. JETP **7** (1958) 505.

- [3] Y. Nambu and G. Jona-Lasinio, Phys. Rev. **122** (1961) 345; *ibid* **124** (1961) 246.
- [4] B.C. Barrois, Nucl. Phys. **B129** (1977) 390;
D. Bailin and A. Love, Phys. Rep. **107** (1984) 325;
M. Alford, K. Rajagopal and F. Wilczek, Phys. Lett. **B422** (1998) 247; Nucl. Phys. **B537** (1999) 443;
R. Rapp, T. Schäfer, E.V. Shuryak and M. Velkovsky, Phys. Rev. Lett. **81** (1998) 53.
- [5] J. Berges and K. Rajagopal, Nucl. Phys. **B538** (1999) 215.
- [6] R.D. Pisarski and D.H. Rischke, Phys. Rev. **D60**:094013 (1999); *ibid* **D61**:051501 (2000); **D61**:074017 (2000).
- [7] J.B. Kogut, M.A. Stephanov, D. Toublan, J.J.M. Verbaarschot and A. Zhitnitsky, Nucl. Phys. **B582** (2000) 477.
- [8] S.J. Hands, I. Montvay, S.E. Morrison, M. Oevers, L. Scorzato and J. Skullerud, Eur. Phys. J. **C17** (2000) 285.
- [9] J.B. Kogut, D.K. Sinclair, S.J. Hands and S.E. Morrison, hep-lat/0105026.
- [10] I.M. Barbour, S.J. Hands, J.B. Kogut, M.-P. Lombardo and S.E. Morrison, Nucl. Phys. **B557** (1999) 327.
- [11] S.J. Hands, S. Kim and J.B. Kogut, Nucl. Phys. **B442** (1995) 364.
- [12] D.R. Tilley and J. Tilley, *Superfluidity and Superconductivity*, (Adam Hilger, Bristol, 1990).
- [13] N.W. Ashcroft and N.D. Mermin, *Solid State Physics*, (Holt, Rinehart and Winston, New York, 1976).
- [14] G.E. Volovik, *Exotic Properties of Superfluid ^3He* (World Scientific, Singapore, 1992).
- [15] S.J. Hands and S.E. Morrison, Phys. Rev. **D59**:116002 (1999).
- [16] S.J. Hands, B. Lucini and S.E. Morrison, Phys. Rev. Lett. **86** (2001) 753.
- [17] B. Rosenstein, B.J. Warr and S.H. Park, Phys. Rep. **205** (1991) 59.

- [18] S.J. Hands, A. Kocić and J.B. Kogut, *Ann. Phys. (N.Y.)* **224** (1993) 29.
- [19] D.R. Nelson and J.M. Kosterlitz, *Phys. Rev. Lett.* **39** (1977) 1201;
D.R. Nelson, in *Phase Transitions and Critical Phenomena*, Vol **7** (1983) p.1,
eds. C. Domb and J.L. Lebowitz (Academic Press, London).
- [20] J.M. Kosterlitz and D.J. Thouless, *J. Phys.* **C6** (1973) 1181.
- [21] L.D. Landau, *Sov. Phys. JETP* **3** (1956) 920; *ibid* **5** (1957) 101.
- [22] E.M. Lifshitz and L.P. Pitaevskii, *Statistical Physics (Part 2)* (Landau and Lifshitz Vol. 9) (Pergamon Press, Oxford 1980).
- [23] S.J. Hands and J.B. Kogut, *Nucl. Phys.* **B520** (1998) 382.
- [24] B. Rosenstein, B.J. Warr and S.H. Park, *Phys. Rev.* **D39** (1989) 3088;
S.J. Hands, A. Kocić and J.B. Kogut, *Nucl. Phys.* **B390** (1993) 355;
A.S. Vshivtsev, B.V. Magnitskii, V.Ch. Zhukovskii and K.G. Klimenko, *Phys. Part. Nucl.* **29** (1998) 523.
- [25] J.B. Kogut and C.G. Strouthos, *Phys. Rev.* **D63**:054502 (2001).
- [26] C.J. Burden and A.N. Burkitt, *Europhys. Lett.* **3** (1987) 545.
- [27] S. Gottlieb, W. Liu, D. Toussaint, R.L. Renken and R. Sugar, *Phys. Rev.* **D35** (1987) 2531.
- [28] S.-K. Ma, *Modern Theory of Critical Phenomena*, (Benjamin, Reading MA, 1976).
- [29] L. Del Debbio, S.J. Hands and J.C. Mehegan, *Nucl. Phys.* **B502** (1997) 269.
- [30] A. Kocić, J.B. Kogut and K.C. Wang, *Nucl. Phys.* **B398** (1993) 405.
- [31] N.D. Mermin and H. Wagner, *Phys. Rev. Lett.* **17** (1966) 1133;
S. Coleman, *Comm. Math. Phys.* **31** (1973) 259.
- [32] P.C. Hohenberg, *Phys. Rev.* **158** (1967) 383.
- [33] V.L. Berezinskii, *Sov. Phys. JETP* **34** (1972) 610.
- [34] K. Iida and G. Baym, [hep-ph/0108149](#).

- [35] J.M. Kosterlitz, J. Phys. **C7** (1974) 1046.
- [36] S.J. Hands, J.B. Kogut and C.G. Strouthos, Phys. Lett. **B515** (2001) 407.
- [37] J.A. Gracey, Int. J. Mod. Phys. **A6** (1991) 395; *ibid* **A9** (1994) 567, Phys. Rev. **D50** (1994) 2840;
 L. Kärkkäinen, R. Lacaze, P. Lacock and B. Petersson, Nucl. Phys. **B415** (1994) 781;
 E. Focht, J. Jersák and J. Paul, Phys. Rev. **D53** (1996) 4616;
 S.J. Hands and B. Lucini, Phys. Lett. **B461** (1999) 263.
- [38] G. Baym and S.A. Chin, Nucl. Phys. **A262** (1976) 527.
- [39] J. Kapusta and T. Toimela, Phys. Rev. **D37** (1988) 3731.
- [40] S.J. Hands, J.B. Kogut, C.G. Strouthos and T.N. Tran, in preparation.
- [41] K. Langfeld, H. Reinhardt and M. Rho, Nucl. Phys. **A622** (1997) 620;
 K. Langfeld, Nucl. Phys. **A642** (1998) 96c.
- [42] S.P. Klevansky, Rev. Mod. Phys. **64** (1992) 649.